Geophysical Journal International

A model of elastic softening and second order phase transitions in anisotropic phases, with application to stishovite and post-stishovite

Journal:	*Geophysical Journal International*
Manuscript ID	GJI-24-0478
Manuscript Type:	Research Paper
Date Submitted by the Author:	03-Aug-2024
Complete List of Authors:	Myhill, Robert; University of Bristol, School of Earth Sciences
Keywords:	Equations of state < COMPOSITION and PHYSICAL PROPERTIES, Seismic anisotropy < SEISMOLOGY, Elasticity and anelasticity < COMPOSITION and PHYSICAL PROPERTIES

submitted to *Geophys. J. Int.*

A model of elastic softening and second order phase transitions in anisotropic phases, with application to stishovite and post-stishovite

R. Myhill[1]⋆

[1]*School of Earth Sciences, University of Bristol. Wills Memorial Building, Queen's Road, Bristol BS8 1RJ*

SUMMARY

This paper presents a framework for describing instantaneous and time-dependent elastic softening in anisotropic solid solutions. The framework is based on Landau theory, minimizing a thermodynamic potential by varying isochemical parameters ($\boldsymbol{q}$) that describe changes in structural, ordering or electronic spin state. Unlike previous models, no coupling terms are used; strain is not a parameter involved in the energy minimization, but is instead a property of the material. The framework satisfies all the elastic and thermodynamic identities known as Maxwell's relations. The stishovite to post-stishovite transition is used to illustrate the validity of the formulation. It is shown that around the transition, the stishovite-post stishovite phase is auxetic in many directions and has negative linear compressibility along the long axis of the cell.

Key words: Equations of state – Elasticity and anelasticity – Seismic anisotropy – Elastic softening

⋆ bob.myhill@bristol.ac.uk

1 INTRODUCTION

1.1 Isochemical variability in crystalline materials

The thermodynamic and elastic properties of crystalline phases are generally functions of the numbers of moles of independent chemical species $\boldsymbol{n}$ comprising those phases. In many solutions, phases can be adequately modelled using only independent species that are compositionally independent from each other, such that the vector of independent chemical *components* $\boldsymbol{x}$ and vector of independent chemical *species* $\boldsymbol{n}$ have the same length. For example, $(Mg, Fe)_3Al_2Si_3O_{12}$ garnet (a two-component system, $n_x = 2$) can be reasonably modelled as a mixture of only two species ($n_n = 2$): pyrope $[Mg]_3Al_2Si_3O_{12}$ and almandine $[Fe]_3Al_2Si_3O_{12}$. However, there are many pure phases and solid solutions whose properties can only be modelled accurately by explicitly considering one or more isochemical degrees of freedom $\boldsymbol{q}$.

Three important types of isochemical degrees of freedom are chemical species ordering on crystallographic sites, electronic spin state, and structural flexibility. Examples of each of these, and possible definitions of the corresponding isochemical degree of freedom q (assuming $n_q = 1$) include:

- Ordering: Mg-Si exchange on two distinct octahedral sites in majorite (Heinemann et al., 1997):

$$q = (p_{\mathrm{Mg^{M1}}} + p_{\mathrm{Si^{M2}}}) - (p_{\mathrm{Si^{M1}}} + p_{\mathrm{Mg^{M2}}})$$

- Electronic spin state: Variable proportions of high spin and low spin Fe^{2+} in ferropericlase (Wu et al., 2013) or troilite (Urakawa et al., 2004):

$$q = p_{\mathrm{Fe^M_{HS}}} - p_{\mathrm{Fe^M_{LS}}}$$

- Structural flexibility: Tilt angle Θ of tetrahedral SiO_4-units in quartz (Carpenter et al., 1998; Wells et al., 2002) or albite (Mookherjee et al., 2016), or octahedral SiO_6-units in $CaCl_2$-structured stishovite (Zhang et al., 2023):

$$q = \Theta$$

If $\boldsymbol{q}$ is both an important contributor to the energy of a phase, and is able to adjust on the timescales of changes in stress or temperature, anomalous material properties may be observed (Salje, 1985; Carpenter, 2006).

1.2 Anomalous thermodynamic and elastic properties

One of the earliest observations of anomalous properties associated with isochemical degrees of freedom was seen during the heating of quartz through the displacive α-β transition. Le Chatelier (1890) observed that cell lengths increased rapidly on approaching 570°C, and then decreased above 570°C.

This peculiar behaviour is also associated with elastic softening (Carpenter et al., 1998; Lakshtanov et al., 2007) and a peak in heat capacity (Grønvold & Stølen, 1992). The change in behaviour at 570°C is now known to mark a weak first order trigonal to hexagonal transition (e.g. Antao, 2016). Cooling through this transition leads to alternating tilting of SiO_4 tetrahedra, and both this and dynamic tilting in the high temperature phase (Welche et al., 1998; Wells et al., 2002) lead to the observed anomalies in physical properties.

Since the discovery of the anomalous properties of quartz, anomalous material properties, many but not all associated with phase transitions, have been discovered in many other phases (Helgeson, 1978; Thompson & Perkins, 1981; Wadhawan, 1982; Dove, 1997; Carpenter, 2006). These include some of the most abundant phases in the Earth: feldspar (Mookherjee et al., 2016; Lacivita et al., 2020), garnet (Heinemann et al., 1997), orthopyroxene (Reynard et al., 2010), amphibole (Cámara et al., 2003), cristobalite (Yeganeh-Haeri et al., 1992) stishovite (Carpenter et al., 2000), ferropericlase (Wu et al., 2013) and $CaSiO_3$ perovskite (Stixrude et al., 2007). In all cases, the anomalous properties arise from the presence of one or more isochemical degrees of freedom in the crystalline structure.

1.3 Aim of this paper

Existing methods to model the anomalous properties of elastic materials are either strictly hydrostatic (i.e. only returning bulk modulus rather than the full elastic tensor) (e.g. Angel et al., 2017), or athermal (making no distinction between isothermal and isentropic moduli, and restricted to a single temperature) (e.g. Carpenter & Salje, 1998; Carpenter, 2006). These methods are all based on Landau theory, which explicitly models the effect of isochemical variables on thermodynamic potentials and their derivatives.

In this paper, I show how Landau theory can be extended to self-consistently determine the full set of thermodynamic and elastic properties of anisotropic crystalline phases. The formulation can be applied over geologically relevant pressure and temperature ranges. Both instantaneous and time-dependent relaxation are considered.

Table 1. Symbols used in this paper.

Symbol	Units	Description
$\mathcal{E}$, $\mathcal{F}$, $\mathcal{G}$, $\mathcal{H}$	J	Internal energy, Helmholtz energy, Gibbs energy, Enthalpy
$\boldsymbol{M}$, M_{ij}	m	Metric tensor
$\boldsymbol{F}$, F_{ij}	[unitless]	Deformation gradient tensor
$\boldsymbol{\sigma}$, σ_{ij}	Pa	Cauchy ("true") stress
$\bar{\boldsymbol{\varepsilon}}$, $\bar{\varepsilon}_{ij}$	[unitless]	Non-hydrostatic isochoric small strain tensor
T	K	Temperature
N	J/K	Entropy
V	m^3	Volume
f	[unitless]	Logarithmic volume ($\ln(V/(1m))$)
$\boldsymbol{n}$, n_i	mol	Molar amounts of compositional/structural endmembers
$\boldsymbol{p}$, p_i	[unitless]	Molar proportions of endmembers
$\boldsymbol{q}$, q_i	[unitless]	Isochemical relaxation vectors
$\boldsymbol{x}$, x_i	mol	Molar amounts of compositional/structural endmembers independent of relaxation vectors
$\boldsymbol{\mu}$	J/mol	Chemical potentials of endmembers
P	Pa	Pressure (-$\delta_{ij}\sigma_{ij}/3$)
$\boldsymbol{\pi}$, π_{ij}	Pa/K	Thermal stress tensor
$\mathbb{C}_{\mathrm{T}}$, $\mathbb{C}_{\mathrm{T}ijkl}$, $\mathbb{C}_{\mathrm{T}pq}$	Pa	Isothermal stiffness tensor (standard and Voigt form)
$\mathbb{C}_{\mathrm{N}}$, $\mathbb{C}_{\mathrm{N}ijkl}$, $\mathbb{C}_{\mathrm{N}pq}$	Pa	Isentropic stiffness tensor (standard and Voigt form)
$\boldsymbol{\alpha}$, α_{ij}; α_V	K^{-1}	Thermal expansivity tensor; Volumetric thermal expansivity
$C_{\boldsymbol{\sigma}}$, $C_{\boldsymbol{\varepsilon}}$, C_V, C_P	J/K	Isostress, isometric, hydrostatic-isochoric and isobaric heat capacities
β_{TR}, β_{NR}	Pa^{-1}	Isothermal and isentropic Reuss compressibilities
K_{TR}, K_{NR}	Pa	Isothermal and isentropic Reuss bulk moduli
$\boldsymbol{\gamma}$, γ_{ij}	[unitless]	Grüneisen tensor
Ψ, Ψ_{ijkl}	[unitless]	Anisotropic state tensor
$\boldsymbol{I}$, δ_{ij}		Identity matrix / Kronecker delta
$\ln_{\mathrm{M}}()$		Matrix logarithm function
$\exp_{\mathrm{M}}()$		Matrix exponential function

2 LANDAU THEORY

2.1 Previous Landau formulations of structurally flexible lattices

In the 1930s, Landau wrote a series of papers designed to explain anomalous peaks in heat capacity (Landau, 1935) and other phenomena involving continuous transitions (those without a finite release of latent heat over an infinitesimal temperature range) (Landau, 1937a,b). See English translations in (Landau, 2008; Ter Haar, 2013). The basic idea behind Landau's method is to model the excess energy Φ_{xs} as a polynomial in $\boldsymbol{q}$:

$$\Phi_{\text{xs}} = a_i q_i + b_{ij} q_i q_j + c_{ijk} q_i q_j q_k + \dots \tag{1}$$

where a_i, b_{ij}, c_{ijk}, ... are all potentially functions of the natural variables of Φ. Landau implicitly used the Gibbs energy ($\mathcal{G}(P, T, \boldsymbol{x})$; e.g. Landau, 1935) and Helmholtz energy ($\mathcal{F}(V, T, \boldsymbol{x})$; e.g. Landau & Ginzburg, 1950) as convenient energies for different problems. The equilibrium state $\boldsymbol{q}^*$ at any given state can be found by minimizing Φ while holding the other natural variables constant. Continuous symmetry-breaking phase transitions (Wadhawan, 1982) arise naturally at conditions where $\Phi(q)$ curves transition from being concave down (stable equilibrium points) to concave up (metastable equilibrium points).

The original Landau models were designed only to investigate the scalar properties of materials, such as entropy and volume, heat capacity and bulk modulus. In order to study unit cell changes and elasticity at fixed bulk composition, Devonshire (1949) and Lüthi & Rehwald (1981) introduced modified Landau models where the elements of the strain tensor $\boldsymbol{\varepsilon}$ were included as additional order parameters:

$$\mathcal{F}(V, T, \boldsymbol{q}, \boldsymbol{\varepsilon}) = \mathcal{F}_{\text{ref}}(V, T) + \mathcal{F}_{\text{xs}}(V, T, \boldsymbol{q}, \boldsymbol{\varepsilon}) \tag{2}$$

$$\mathcal{F}_{\text{xs}}(V, T, \boldsymbol{q}, \boldsymbol{\varepsilon}) = a_i q_i + b_{ij} q_i q_j + c_{ijk} q_i q_j q_k + \dots + \sum_{ij,m,n} \lambda_{ij,k,m} \varepsilon_i^m q_j^n + \frac{1}{2} V \sum_{i,k} \mathbb{C}^0_{ik} \varepsilon_i \varepsilon_k \tag{3}$$

In this expression, a, b, c, $\lambda_{ij,k,m}$, C^0_{ik}, ... are all potentially functions of volume and temperature, and C^0_{ik} may additionally be a function of $\boldsymbol{q}$. The terms before the "..." are those found in the scalar Landau model (Equation 1), the penultimate term is a "strain-order" coupling term, and the last term is an elastic term. The penultimate term allows changes in the structure parameters $\boldsymbol{q}$ to "drive" structural strain. Devonshire (1949) assigned the order parameters $\boldsymbol{q}$ to be equal to the three components of the electrical polarisation vector $\boldsymbol{P}$.

Expansions in both the Helmholtz and Gibbs energy like Equation 3 have been extensively used to investigate phase transitions (Carpenter & Salje, 1998; Carpenter et al., 1998, 2000; Carpenter, 2006; Kityk et al., 2000; Liakos & Saunders, 1982; Schranz et al., 2007; Tröster et al., 2002, 2014, 2017; Buchen, 2021). The conceptual problem with such models is that under hydrostatic conditions in the

absence of electrical order magnetic fields, P (or V), T, $\boldsymbol{x}$ and $\boldsymbol{q}$ are the only independent variables. Strain and polarisation are not independent variables, and as a result, Landau minimizations treating them as free parameters will generally be thermodynamically inconsistent. In the case of Equation 3, there are three potential sources of inconsistency:

- $\det(\boldsymbol{\varepsilon})$ should be equal to zero if V is used as an independent variable, but minimizations do not enforce this constraint. Therefore, the Landau minimization must also solve for V, or minimization must be constrained to ensure that $\det(\boldsymbol{\varepsilon}) = 0$.
- The "bare" elastic parameters $\mathbb{C}^0$ should satisfy the hydrostatic (Reuss), isothermal bulk modulus K_{TR}, because of the following thermodynamic constraint:

$$K_{\mathrm{TR}} = V\left(\frac{\partial^2 \mathcal{F}}{\partial V \partial V}\right)_{T,\boldsymbol{q}} = \frac{1}{\boldsymbol{I}(\mathbb{C}^0_{T,\boldsymbol{q}})^{-1}\boldsymbol{I}} \tag{4}$$

but minimizations do not enforce this constraint.

- $\boldsymbol{\varepsilon}$ is typically assumed to be the *engineering strain tensor*, but $V\mathbb{C}_{\mathrm{T}}$ is the second partial derivative of the Helmholtz energy with respect to *infinitesimal strain*. Partial derivatives with respect to these two tensors are only equivalent for infinitesimal strains, but the strains involved in symmetry-breaking transitions (relative to the state at $\boldsymbol{q} = \boldsymbol{0}$) are often quite large. Therefore, taking the second derivative of $\mathcal{F}$ with respect to $\boldsymbol{\varepsilon}$ only provides a first-order approximation to the true elasticity tensor.

More pragmatically, even if we do not care about thermodynamic consistency, it would be convenient to be able to use scalar Landau models (where minimization is performed only over the isochemical variables $\boldsymbol{q}$) to study elastic, polarisation and magnetic anomalies.

2.2 An alternative Landau formulation

In a companion paper (Myhill, 2024), I proposed a self-consistent model of thermoelastic properties in solid solutions. In that paper, the Helmholtz energy, cell tensor and the elastic properties under hydrostatic conditions were expressed as a function of V, T, independent endmember amounts $\boldsymbol{n}$ and an isochoric (constant volume) small strain tensor $\bar{\boldsymbol{\varepsilon}}$:

$$\mathcal{F}(V,T,\boldsymbol{n},\bar{\boldsymbol{\varepsilon}}) = \mathcal{F}_{\mathrm{hyd}}(V,T,\boldsymbol{n}) + \mathcal{F}_{\mathrm{el}}(V,T,\boldsymbol{n},\bar{\boldsymbol{\varepsilon}}) \tag{5}$$

$$M_{ij}(V,T,\boldsymbol{n},\bar{\boldsymbol{\varepsilon}}) = (\delta_{ik} + \bar{\varepsilon}_{ik})F_{kl}(V,T,\boldsymbol{n})M_{0lj}(\boldsymbol{n}) \tag{6}$$

$$\mathcal{F}_{\mathrm{el}}(V,T,\boldsymbol{n},\bar{\boldsymbol{\varepsilon}}) = \frac{1}{2}V\sum_{i,j}\bar{\varepsilon}_i\mathbb{C}_{\mathrm{T,hyd}ij}(V,T,\boldsymbol{n})\bar{\varepsilon}_j \tag{7}$$

A linear transformation can be applied to the endmember amounts vector $\boldsymbol{n}$, splitting it into a set of isochemical "order parameters" $\boldsymbol{q}$ and other linearly independent vectors $\boldsymbol{x}$ (Myhill & Connolly, 2021). The change in $\boldsymbol{n}$ resulting from changes in $\boldsymbol{q}$ and $\boldsymbol{x}$ can be described by the following linear

relation

$$dn_i = A_{ij} dq_j + B_{ik} dx_k \tag{8}$$

where $\boldsymbol{A}$ and $\boldsymbol{B}$ are constant transformation matrices. This division allows the solution model to be transformed into a form conducive to Landau theory:

$$\mathcal{F}(V, T, \boldsymbol{x}, \boldsymbol{q}, \bar{\boldsymbol{\varepsilon}}) = \mathcal{F}_{\text{hyd}}(V, T, \boldsymbol{x}, \boldsymbol{q}) + \mathcal{F}_{\text{el}}(V, T, \boldsymbol{x}, \boldsymbol{q}, \bar{\boldsymbol{\varepsilon}}) \tag{9}$$

$$M_{ij}(V, T, \boldsymbol{x}, \boldsymbol{q}, \bar{\boldsymbol{\varepsilon}}) = (\delta_{ik} + \bar{\varepsilon}_{ik}) F_{kl}(V, T, \boldsymbol{x}, \boldsymbol{q}) M_{0lj}(\boldsymbol{x}, \boldsymbol{q}) \tag{10}$$

$$\mathcal{F}_{\text{el}}(V, T, \boldsymbol{x}, \boldsymbol{q}, \bar{\boldsymbol{\varepsilon}}) = \frac{1}{2} V \sum_{i,j} \bar{\varepsilon}_i \mathbb{C}_{\text{T,hyd}ij}(V, T, \boldsymbol{x}, \boldsymbol{q}) \bar{\varepsilon}_j \tag{11}$$

The hydrostatic part of the Helmholtz energy can also be calculated from the Gibbs energy, if pressure is a more convenient independent variable than volume:

$$\mathcal{F} = \mathcal{G}_{\text{hyd}}(P, T, \boldsymbol{x}, \boldsymbol{q}) - P\,V(P, T, \boldsymbol{x}, \boldsymbol{q}) \tag{12}$$

$$V = \frac{\partial \mathcal{G}_{\text{hyd}}}{\partial P} \tag{13}$$

The benefits of this formalism over Equation 3 are:

- Landau energy minimization can be performed by varying $\boldsymbol{q}$, and not strain, polarisation or magnetic moment.
- The cell tensor $\boldsymbol{M}$ and isothermal elastic stiffness tensor $\mathbb{C}_{\text{T}}$ are always consistent with the volume.
- The strain tensor $\bar{\boldsymbol{\varepsilon}}$ is strictly infinitesimal and isochoric, and so hyperelasticity does not need to be considered.

Table 2. Variable sets used in this paper. For the meaning of each variable, see Table 1.

Set	Identifier	Independent variables	Section of first appearance
Helmholtz ("natural")	$\ldots$	$\boldsymbol{M}$, T, $\boldsymbol{n}$	3.2
"Relaxed" Helmholtz	$\ldots^*$	$\boldsymbol{M}$, T, $\boldsymbol{x}$, $\boldsymbol{q}$	3.3.1
Anisotropic EoS	$\ldots'$	V, T, $\boldsymbol{n}$, $\bar{\boldsymbol{\varepsilon}}$	3.3.2
Gibbs energy (hydrostatic)	$\ldots^{\mathcal{G}}$	P, T, $\boldsymbol{n}$	3.3.2
Internal energy	$\ldots^{\mathcal{E}}$	$\boldsymbol{M}$, N, $\boldsymbol{n}$	3.4

3 MATERIAL PROPERTIES UNDER UNRELAXED, RELAXED AND TIME-DEPENDENT RELAXING STATES

3.1 Natural variables, properties and relaxation in elastic materials

Under strictly hydrostatic conditions, the natural variables of a system can be chosen to be pressure P or volume V, entropy N or temperature T, and the number of moles of chemical species $\boldsymbol{n}$ or their chemical potentials $\boldsymbol{\mu}$. The exact choice dictates which thermodynamic energy is minimized at equilibrium to satisfy the second law of thermodynamics: for example, at fixed pressure and temperature the Gibbs energy $\mathcal{G}(P,T,\boldsymbol{n})$ is minimized. Other energies used in this study are the internal energy $\mathcal{E}(V,N,\boldsymbol{n})$ and Helmholtz energy $\mathcal{F}(V,N,\boldsymbol{n})$.

If the stress is allowed to be non-hydrostatic, the pressure or volume are insufficient to completely determine the state of a material, and they must be replaced by the stress or some measure of strain as natural variables. It is often convenient to use different natural variables for different tasks: pressure and temperature are the most suitable natural variables for geological state, but strain and entropy are the most suitable for seismic propagation. In this study, a number of variable sets are used (Table 2).

Whichever variables are chosen, the thermodynamic and elastic properties of a material can be determined from partial derivatives of the thermodynamic energies. Derivatives of the Helmholtz energy are given in Section 3.2. As already mentioned in Section 1.2, all of these properties are potentially a function of the isochemical variables $\boldsymbol{q}$. Second derivatives of the thermodynamic energies are particularly interesting because they not only depend on $\boldsymbol{q}$, but also on how $\boldsymbol{q}$ changes as the natural variables change. In this paper, material properties are referred to as "unrelaxed" if $\boldsymbol{q}$ is not allowed to vary as the natural variables change, and "relaxed" if $\boldsymbol{q}$ responds rapidly to minimize energy compared with the timescales over which the natural variables change. Unrelaxed properties, relaxed properties and partially relaxed behaviour are covered separately in Sections 3.2, 3.3 and 3.4.

3.2 The properties of an unrelaxed elastic material

3.2.1 Derivatives of the Helmholtz energy

The Helmholtz energy of a homogeneously strained crystalline material can be written $\mathcal{F} = \mathcal{F}(\boldsymbol{M}, T, \boldsymbol{n})$, a function of the unit cell tensor $\boldsymbol{M}$, temperature T and amount of different chemical species $\boldsymbol{n}$. First derivatives of the natural variables define the Cauchy stress $\boldsymbol{\sigma}$, entropy N and chemical potentials μ_i:

$$d\mathcal{F} = \frac{\partial \mathcal{F}}{\partial \varepsilon_{ij}} d\varepsilon_{ij} + \frac{\partial \mathcal{F}}{\partial T} dT + \frac{\partial \mathcal{F}}{\partial n_i} dn_i \tag{14}$$

$$= V\sigma_{ij} d\varepsilon_{ij} - N dT + \mu_i dn_i \tag{15}$$

$$d\varepsilon_{ij} = \frac{1}{2}(dM_{ik} M^{-1}_{jk} + dM_{jk} M^{-1}_{ik}) \tag{16}$$

where $\boldsymbol{\varepsilon}$ is the small strain tensor. The work term can be further split into volumetric and rotation-free, isochoric strain $\bar{\boldsymbol{\varepsilon}}$ (Holzapfel, 2000):

$$d\mathcal{F} = -P dV + V\tau_{ij} d\bar{\varepsilon}_{ij} - N dT + \mu_i dn_i \tag{17}$$

The second derivatives of the Helmholtz energy with respect to strain and temperature at fixed $\boldsymbol{n}$ (Equation 15) yield the isothermal stiffness tensor ($\mathbb{C}_{\mathrm{T}}$), the thermal stress tensor ($\boldsymbol{\pi}$) and the isometric heat ($c_{\boldsymbol{\varepsilon}}$):

$$\left(\frac{\partial^2 \mathcal{F}}{\partial \varepsilon_{ij} \partial \varepsilon_{kl}}\right)_{\boldsymbol{n}, T, \varepsilon_{mn \neq ij,kl}} = V \mathbb{C}_{\mathrm{T}ijkl} \tag{18}$$

$$\left(\frac{\partial^2 \mathcal{F}}{\partial \varepsilon_{ij} \partial T}\right)_{\boldsymbol{n}, \varepsilon_{kl \neq ij}} = V \pi_{ij} \tag{19}$$

$$\left(\frac{\partial^2 \mathcal{F}}{\partial T \partial T}\right)_{\boldsymbol{n}, \boldsymbol{\varepsilon}} = -\frac{c_{\boldsymbol{\varepsilon}}}{T} \tag{20}$$

3.2.2 Other thermodynamic properties

Other thermodynamic properties may be determined through appropriate algebraic manipulation of these properties (Davies, 1974; Nye et al., 1985; Holzapfel, 2000):

$$\mathbb{C}_{\mathrm{N}} = \mathbb{C}_{\mathrm{T}} + \frac{VT}{c_{\boldsymbol{\varepsilon}}} \boldsymbol{\pi}\boldsymbol{\pi} \tag{21}$$

$$\mathbb{S}_{\mathrm{T}} = (\mathbb{C}_{\mathrm{T}})^{-1}; \quad \mathbb{S}_{\mathrm{N}} = (\mathbb{C}_{\mathrm{N}})^{-1} \tag{22}$$

$$\beta_{\mathrm{TR}} = \boldsymbol{I}\mathbb{S}_{\mathrm{T}}\boldsymbol{I}; \quad \beta_{\mathrm{NR}} = \boldsymbol{I}\mathbb{S}_{\mathrm{N}}\boldsymbol{I} \tag{23}$$

$$\boldsymbol{\alpha} = -\mathbb{S}_{\mathrm{T}}\boldsymbol{\pi}; \quad \alpha_V = \mathrm{Tr}(\boldsymbol{\alpha}) \tag{24}$$

$$c_{\boldsymbol{\sigma}} = c_{\boldsymbol{\varepsilon}} + VT\boldsymbol{\alpha}\mathbb{C}_{\mathrm{T}}\boldsymbol{\alpha} = c_{\boldsymbol{\varepsilon}} - VT\boldsymbol{\alpha}\boldsymbol{\pi} \tag{25}$$

$$\boldsymbol{\gamma} = \mathbb{C}_{\mathrm{N}}\boldsymbol{\alpha}\frac{V}{c_{\boldsymbol{\sigma}}} \tag{26}$$

Under hydrostatic conditions, the following scalar properties can be defined:

$$c_P = c_{\boldsymbol{\sigma}} = \frac{VT\alpha_V^2}{(\beta_{\text{TR}} - \beta_{\text{NR}})} \tag{27}$$

$$c_V = c_P - VT\frac{\alpha_V^2}{\beta_{\text{TR}}} \tag{28}$$

$$\gamma = \frac{\alpha V}{\beta_{\text{NR}} c_P} \tag{29}$$

3.3 The properties of a rapidly relaxed elastic material

3.3.1 Variational calculus

The expressions for the second derivatives of the Helmholtz energy in Section 3.2 (Equations 18, 19 and 20) assume that none of the isochemical structural parameters $\boldsymbol{q}$ incorporated into $\boldsymbol{n}$ (Section 2.2) change on the timescales of perturbations in $\boldsymbol{\varepsilon}$ or T. However, spin transitions and spontaneous flexure/rotation of structural units are often considered to be essentially instantaneous on seismic timescales (Slonczewski & Thomas, 1970; Zhang et al., 2018). For example, the relaxation of quartz tetrahedral tilts takes place on nanosecond or even picosecond timescales (Kimizuka et al., 2003). In the endmember scenario that one or more isochemical order parameters $\boldsymbol{q}$ change instantaneously to minimize $\mathcal{F}$ under small changes in strain and temperature, variational calculus can be used to calculate relaxed properties, marked in this paper by an asterisk *. Relaxed values of $\boldsymbol{q}$ are therefore a function of the other variables of the system:

$$\boldsymbol{q}^* = \boldsymbol{q}^*(\boldsymbol{M}, T, \boldsymbol{x}) \tag{30}$$

For small, rotation-free perturbations about a hydrostatic state $\boldsymbol{M}_0$ (such that $\boldsymbol{M} = (\boldsymbol{I} + \boldsymbol{\varepsilon})\boldsymbol{M}_0$), we can consider the small strain tensor only

$$\boldsymbol{q}^* = \boldsymbol{q}^*(\boldsymbol{\varepsilon}, T, \boldsymbol{x}) \tag{31}$$

Ignoring $\boldsymbol{x}$ (which cannot change without breaking bonds), and collecting small strain and temperature together as $\boldsymbol{z} = \{\boldsymbol{\varepsilon}, T\}$, the change in $\boldsymbol{q}^*$ with change in $\boldsymbol{z}$ can be determined using the following expression (Appendix A):

$$\frac{\partial q_k^*}{\partial z_j} = -R_{kl}\frac{\partial^2 \mathcal{F}}{\partial q_l \partial z_j} \tag{32}$$

where $\boldsymbol{R}$ is the left inverse matrix of $\partial^2\mathcal{F}/\partial q_l \partial q_m$:

$$\delta_{km} = R_{kl}\frac{\partial^2 \mathcal{F}}{\partial q_l \partial q_m} \tag{33}$$

The relationship between the relaxed and unrelaxed second derivatives of the Helmholtz energy with respect to state is then given by the following expressions:

$$\frac{\partial^2 \mathcal{F}^*}{\partial z_i \partial z_j} = \frac{\partial^2 \mathcal{F}}{\partial z_i \partial z_j} + \frac{\partial^2 \mathcal{F}}{\partial z_i \partial q_k} \frac{\partial q_k^*}{\partial z_j} \tag{34}$$

$$\left[\begin{array}{c|c} V\mathbb{C}_{\mathrm{T}}^* & V\boldsymbol{\pi}^* \\ \hline V\boldsymbol{\pi}^{*\mathrm{T}} & -C_{\boldsymbol{\varepsilon}}^*/T \end{array}\right]_{ij} = \left[\begin{array}{c|c} V\mathbb{C}_{\mathrm{T}} & V\boldsymbol{\pi} \\ \hline V\boldsymbol{\pi}^{\mathrm{T}} & -c_{\boldsymbol{\varepsilon}}/T \end{array}\right]_{ij} + \frac{\partial^2 \mathcal{F}}{\partial z_i \partial q_k} \frac{\partial q_k^*}{\partial z_j} \tag{35}$$

The values of $\boldsymbol{q}^*$ (Equation 31) are state properties; they have unique values as a function of $\boldsymbol{\varepsilon}$, T, $\boldsymbol{x}$ and do not depend on the path taken to achieve that state. Therefore, the properties calculated in Equation 35, which correspond to properties at fixed strain and temperature can be used in combination with the equations in Section 3.2.2 to determine other relaxed properties at fixed entropy or stress. For example, the equation for the relaxed isentropic stiffness tensor:

$$\mathbb{C}_{\mathrm{N}}^* = \mathbb{C}_{\mathrm{T}}^* + \frac{VT}{c_{\boldsymbol{\varepsilon}}^*} \boldsymbol{\pi}^* \boldsymbol{\pi}^* \tag{36}$$

can be directly compared to the unrelaxed expression (Equation 21).

3.3.2 Change of variables

Equations 32, 33 and 35 require the derivatives of $\mathcal{F}$ with respect to $\boldsymbol{\varepsilon}$, T and $\boldsymbol{q}$, but the equation of state from Myhill (2024) is expressed as $\mathcal{F}(V', T', \boldsymbol{n}', \bar{\boldsymbol{\varepsilon}}')$, where the "primes" are used in this section to differentiate between sets of variables. The required derivatives can be calculated by a change of variables (Appendix B):

$$\frac{\partial^2 \mathcal{F}}{\partial q_i \partial q_j} = A_{ui} \left(H_{uv}^{\mathcal{F}} + V \frac{\partial \varepsilon_{mn}}{\partial n_u'} \mathbb{C}_{\mathrm{T}mnpq} \frac{\partial \varepsilon_{pq}}{\partial n_v'} \right) A_{vj} \tag{37}$$

$$\frac{\partial^2 \mathcal{F}}{\partial q_i \partial T} = A_{ui} \left(-\frac{\partial N}{\partial n_u'} + V \frac{\partial \varepsilon_{mn}}{\partial n_u'} \mathbb{C}_{\mathrm{T}mnpq} \left(\frac{\alpha_{pq}}{\alpha_V} - \frac{\beta_{\mathrm{T}pq}}{\beta_{\mathrm{TR}}} \right) \alpha_V \right) \tag{38}$$

$$\frac{\partial^2 \mathcal{F}}{\partial q_i \partial \varepsilon_{kl}} = -V A_{ui} \left(\delta_{kl} \frac{\partial P}{\partial n_u'} + \frac{\partial \varepsilon_{mn}}{\partial n_u'} \mathbb{C}_{\mathrm{T}mnpq} \left(\delta_{pk}\delta_{ql} - \frac{\beta_{\mathrm{T}pq}}{\beta_{\mathrm{TR}}} \delta_{kl} \right) \right) \tag{39}$$

where

$$\frac{\partial \varepsilon_{mn}}{\partial n_u'} = \frac{1}{2} \left(\frac{\partial M_{mp}}{\partial n_u'} M_{np}^{-1} + \frac{\partial M_{np}}{\partial n_u'} M_{mp}^{-1} \right) \tag{40}$$

Appendix C provides a expression for $\partial \boldsymbol{M} / \partial \boldsymbol{n}'$ using the formulation of the anisotropic equation of state. If the scalar solution equation of state is defined as a function of pressure and temperature (i.e. in terms of the Gibbs energy $\mathcal{G}(P^{\mathcal{G}}, T^{\mathcal{G}}, \boldsymbol{n}^{\mathcal{G}})$), then the following additional conversions are required

(Appendix D):

$$\frac{\partial P}{\partial n'_i} = \frac{K_T}{V}\frac{\partial V}{\partial n_i^{\mathcal{G}}} \tag{41}$$

$$\frac{\partial N}{\partial n'_i} = \frac{\partial N}{\partial n_i^{\mathcal{G}}} - \alpha_V K_T \frac{\partial V}{\partial n_i^{\mathcal{G}}} \tag{42}$$

$$\frac{\partial^2 \mathcal{F}}{\partial n'_i \partial n'_j} = \frac{\partial^2 \mathcal{G}}{\partial n_i^{\mathcal{G}} \partial n_j^{\mathcal{G}}} + \frac{\partial V}{\partial n_i^{\mathcal{G}}}\left(\frac{K_T}{V}\right)\frac{\partial V}{\partial n_j^{\mathcal{G}}} \tag{43}$$

3.4 Time-dependent seismic relaxation

Characteristic timescales of relaxation may be much greater than those involving tilting of structural units or electronic changes. For example, order-disorder processes are often sluggish on seismic timescales, when the activation energy required for migration of species is of larger magnitude than the average thermal energy of those species (Seifert & Virgo, 1975; Ganguly, 1982; Redfern, 1998; Redfern et al., 1999; Redfern, 2000).

If the timescales of relaxation are comparable with the timescales of perturbations in strain, the expressions in Section 3.2 and 3.3 will not correctly predict effective material properties. A simple process of relevance to the Earth Sciences is the passage of a seismic wave, which may be approximated as a periodic perturbation in strain through a single crystal held at constant entropy (thermal diffusion and other entropy-producing processes are inhibited). We assume that relaxation of each structural parameter q_i is driven by the gradient in the internal energy $\mathcal{E}$ with respect to that parameter (analogous to Redfern et al., 1999, replacing the Gibbs energy with the internal energy):

$$\frac{\partial q_i}{\partial t} = -\frac{1}{\lambda_i}\frac{\partial \mathcal{E}}{\partial q_i} \tag{44}$$

In this expression, λ_i represents a thermal time constant with units [K/J]. In the limit of small strains (and therefore small changes in $\boldsymbol{q}$), the energy gradient can be approximated as linear in ε and $\boldsymbol{q}$:

$$\frac{\partial q_i}{\partial t} = -\frac{1}{\lambda_i}\left(\frac{\partial^2 \mathcal{E}}{\partial q_i \partial \varepsilon_{jk}}\varepsilon_{jk} + \frac{\partial^2 \mathcal{E}}{\partial q_i \partial q_j}(q_j - q_{j0})\right) \tag{45}$$

This is a non-homogeneous linear system of equations

$$\frac{\partial x_i(t)}{\partial t} = A_{ij}x_j(t) + b_i(t) \tag{46}$$

where

$$x_i = q_i - q_{i0} \tag{47}$$

$$A_{ij} = -\frac{1}{\lambda_i}\frac{\partial^2 \mathcal{E}}{\partial q_i \partial q_j} \tag{48}$$

$$b_i(t) = -\frac{1}{\lambda_i}\frac{\partial^2 \mathcal{E}}{\partial q_i \partial \varepsilon_{jk}}\varepsilon_{jk}(t) \tag{49}$$

If there is only one parameter q, the behaviour of q is analogous to the deformation of a forced Kelvin-Voigt body (a viscous dashpot in parallel with a spring). For multiple order parameters $\boldsymbol{q}$ and constant matrix $\boldsymbol{A}$ (i.e. for small deformations), the solution to the non-homogeneous system of equations is (Coddington & Levinson, 1984, p78):

$$\boldsymbol{x} = \exp_{\mathrm{M}}(\boldsymbol{A}(t-t_0))\boldsymbol{x}(t_0) + \int_{t_0}^{t} \exp_{\mathrm{M}}(\boldsymbol{A}(t-s))\boldsymbol{b}(s)ds \tag{50}$$

At steady state, a periodic sinusoidal variation in $\boldsymbol{\varepsilon}$ results in a lagged sinusoidal variation in $\boldsymbol{q}$. The change in $\boldsymbol{q}$ drives changes in stress and temperature:

$$\Delta\sigma_{ij} = \mathbb{C}_{\mathrm{N}ijkl}\varepsilon_{kl} + \frac{\partial^2\mathcal{E}}{\partial q_k \partial \varepsilon_{ij}} x_k \tag{51}$$

$$\Delta T = \frac{VT}{c_{\boldsymbol{\varepsilon}}}\pi_{kl}\varepsilon_{kl} + \frac{\partial^2\mathcal{E}}{\partial q_k \partial N} x_k \tag{52}$$

where the thermodynamic properties in the above expressions are evaluated at constant $\boldsymbol{q}$. Analytical expressions for the second order partial derivatives of the internal energy as a function of the partial derivatives of the Helmholtz energy are as follows (Appendix E):

$$\frac{\partial^2\mathcal{E}}{\partial q_i^{\mathcal{E}} \partial N^{\mathcal{E}}} = \frac{T}{c_\varepsilon}\frac{\partial^2\mathcal{F}}{\partial q_i \partial T} \tag{53}$$

$$\frac{\partial^2\mathcal{E}}{\partial q_i^{\mathcal{E}} \partial \varepsilon_{jk}^{\mathcal{E}}} = \frac{\partial^2\mathcal{F}}{\partial q_i \partial \varepsilon_{jk}} + \frac{VT\pi_{jk}}{c_\varepsilon}\frac{\partial^2\mathcal{F}}{\partial q_i \partial T} \tag{54}$$

$$\frac{\partial^2\mathcal{E}}{\partial q_i^{\mathcal{E}} \partial q_j^{\mathcal{E}}} = \frac{\partial^2\mathcal{F}}{\partial q_i \partial q_j} + \frac{\partial^2\mathcal{F}}{\partial q_i \partial T}\frac{T}{c_\varepsilon}\frac{\partial^2\mathcal{F}}{\partial q_j \partial T} \tag{55}$$

4 EXAMPLE: THE STISHOVITE-POST STISHOVITE TRANSITION

4.1 Overview

Stishovite is a high pressure mineral whose composition in natural rocks is dominantly SiO_2. It is stable in mafic and felsic rocks under the *P-T* conditions of the mantle transition zone and the upper part of the lower mantle, an has abundances of around 10-25 wt% of rocks with basaltic compositions (Hirose & Fei, 2002; Holland et al., 2013). It has also been identified in meteorites and their shocked target rocks.

Stishovite experiences a symmetry-breaking displacive phase transition with increasing pressure (Kingma et al. 1995; Andrault et al. 1998). This transition involves the rotation of octahedral SiO_6 groups, transforming stishovite from the tetragonal rutile structure (space group $P4_2/mnm$) to the orthorhombic $CaCl_2$ structure (space group Pnnm). The transition takes place at around 50 GPa at room temperature, and around 78 GPa at 2200 K, which corresponding to a depth of 1800 km depth along a mantle geotherm Brown & Shankland (1981).

At the transition, the a- and b-axes of the stishovite structure become different lengths. Either the a- or the b- axis can become the longer axis, thus allowing the formation of twins with $\{110\}$ as a mirror plane. At the transition, the amount of energy and its derivative required to change from post-stishovite through stishovite to "anti"-post-stishovite is zero, and this results in the isothermal or isentropic sum-of-stiffnesses $\mathbb{C}_{11}$ + $\mathbb{C}_{22}$ - 2$\mathbb{C}_{12}$ dropping to zero, and all of the compliances $\mathbb{S}_{11}$, $\mathbb{S}_{22}$ and $\mathbb{S}_{12}$ approaching infinity from both the low and high pressure sides of the transition. In addition, $\mathbb{S}_{13}$ and $\mathbb{S}_{23}$ approach infinity from the high pressure side of the transition.

Several experimental studies have provided data on the stishovite-post-stishovite transition. This includes unit cell data at high pressure (Andrault et al., 2003; Zhang et al., 2023) and high temperature Ito et al. (1974); Fischer et al. (2018), and also elastic data at high pressure (Zhang et al., 2021b). This data confirm the qualitative elastic predictions of (Carpenter et al., 2000) which were based on early equations of state and the frequency decrease of a Raman-active vibrational mode (Kingma et al., 1995).

All of the papers modelling the elastic anisotropy of the stishovite-post-stishovite transition (Carpenter et al., 2000; Buchen et al., 2018; Buchen, 2021; Zhang et al., 2021b,a, 2022) have used the athermal Landau formalism introduced by (Carpenter & Salje, 1998). Here, I use the available experimental data to parameterise the thermal Landau model described in Section 2.2, and obtain the material properties as derived in Section 3.

4.2 Model formulation

4.2.1 Scalar model

The stishovite - post-stishovite phase can be modelled as a solid solution of post-stishovite ($Q = 1$) and anti-post stishovite ($Q = -1$), where both endmembers have the same properties, but exchanged a and b axes. The displacive second order transition from stishovite to the post-stishovite structure can be modelled by making this solution a "2-4" Landau-type model, where the "2" and "4" indicate that the excess energy of the solution can be modelled as the sum of a $P-T$ dependent quadratic and constant quartic term in the structure parameter Q. Written as a function of the endmember proportions, the excess Gibbs energy is equal to:

$$\mathcal{G}_{\text{xs}} = 4p_0p_1\left((\Delta\mathcal{G}(P,T) - \Delta\mathcal{G}(P_{\text{tr}},T_{\text{tr}})) + 2\Delta\mathcal{G}(P_{\text{tr}},T_{\text{tr}})(p_0^2+p_1^2)\right) \tag{56}$$

$$\Delta\mathcal{G} = \mathcal{G}(P,T,Q=0) - \mathcal{G}(P,T,Q=1) \tag{57}$$

Parameters for the $Q = 0$ and $Q = 1$ states are fit to the data with the equation of state of Stixrude & Lithgow-Bertelloni (2005) (Table 3). To avoid overfitting, only the standard state Helmholtz energy, volume and Debye temperature were allowed to differ between the $Q = 1$ and $Q = 0$ members. These

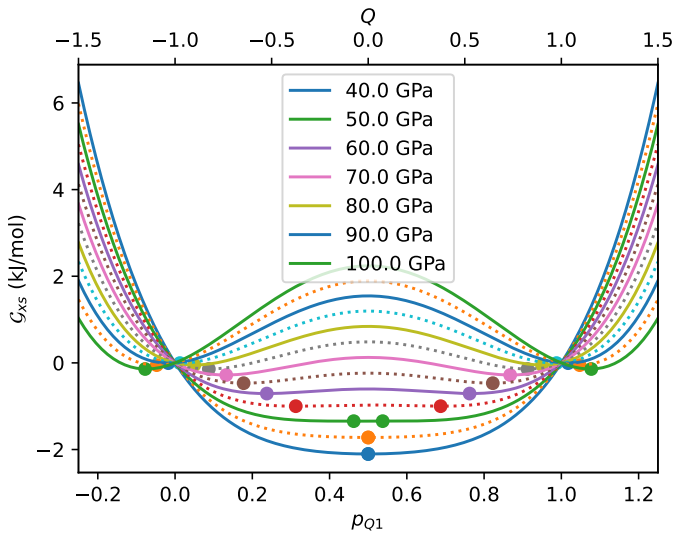

Figure 1. Modelled variation of the excess Gibbs energy relative to post stishovite with $Q = 1$ at a variety of pressures at 298.15 K. The equilibrium value of the structural parameter Q at each pressure is plotted as a single point (before the symmetry-breaking transition) or two points (after the transition).

three properties were chosen because they have a first order influence on the position and slope of the transition, and on the rate of increase of Q with pressure. The absolute value of Q is somewhat arbitrary, so the Helmholtz energy difference was scaled such that a value of $Q = 1$ lay within the pressure range of the data. The resulting parameters lead to a value of $\Delta\mathcal{G}(P_{\text{tr}}, T_{\text{tr}}) = -1361.05$ J/mol. The Gibbs energy as a function of Q at different pressures is shown in Figure 1. The modelled evolution of the equilibrium value of Q is plotted in Figure 2 at a range of pressures and temperatures, and compared with the rotation angle of SiO_6 octahedra about the c-axis from Zhang et al. (2023), which can be used as a proxy for the structural parameter.

4.2.2 Anisotropic model

The anisotropic properties of post-stishovite ($Q = 1$) are modelled via a fourth order tensor Ψ (Section 2.2). After some initial investigation, the following formulation was chosen for the elements of the tensor (given in Voigt form):

$$\Psi_{ij}(f, Q = 1) = (a_{ij} - (b_1c_1 + b_2c_2))f + b_1(\exp(c_1f) - 1) + b_2(\exp(c_2f) - 1) \qquad (58)$$

The available unit cell data at high temperature do not yet support the addition of thermal terms, and there is not yet any elastic tensor data at high temperatures to warrant the use of such terms. The properties of anti-post-stishovite ($Q = -1$) are identical to those of post-stishovite ($Q = 1$), but with the 1st and 2nd rows and columns exchanged, and the 4th and 5th rows and columns exchanged. No

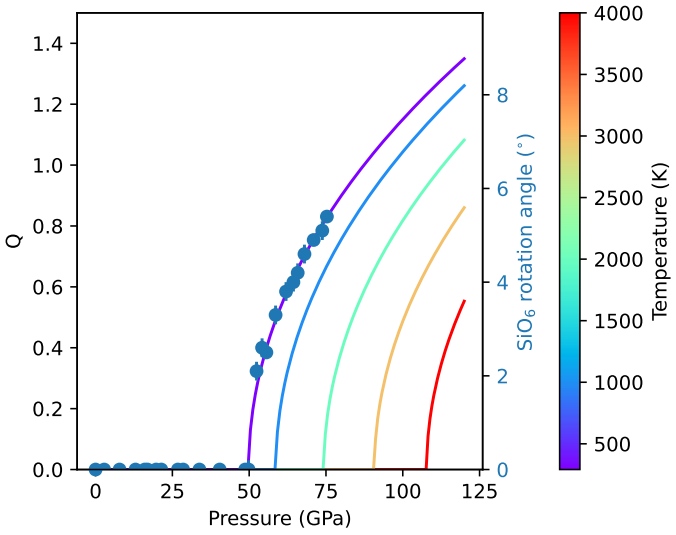

Figure 2. Modelled variation of the equilibrium value of the structural parameter Q in stishovite with respect to pressure and temperature. Values of zero correspond to stishovite, and non-zero values to post-stishovite. Negative values are equally stable, and correspond to "anti"-post-stishovite. Data points correspond to observed SiO_6 rotation angles about the c-axis (Zhang et al., 2023).

excess anisotropic terms are used in the model, so the Ψ tensor for the solution is equal to:

$$\Psi(f,Q) = \left(\frac{1+Q}{2}\right)\Psi(f,Q=1) + \left(\frac{1-Q}{2}\right)\Psi(f,Q=-1) \tag{59}$$

To facilitate data inversion, three further functions are defined (for $i = \{1,2,3\}$):

$$\Psi_i = \Psi_{i1} + \Psi_{i2} + \Psi_{i3} \tag{60}$$

These parameters can be fit using only the a, b and c unit cell vectors, so these functions facilitate the piece-wise inversion scheme described in Section 4.3. If the diagonal elements of Ψ are also fit to the experimental data, the off-diagonals can be determined from:

$$\Psi_{12} = \frac{1}{2}((\Psi_1 + \Psi_2 - \Psi_3) - (\Psi_{11} + \Psi_{22} - \Psi_{33})) \tag{61}$$

4.3 Data processing and inversion

Weighted least squares inversion for the anisotropic properties of stishovite was split into the following stages:

(i) Initial fitting of the $\mathcal{G}(P,T)$ equation of state

(ii) Initial fitting of the unit cell properties $\boldsymbol{M}(V,T,q)$

(iii) Initial fitting of the relaxed elastic moduli $\mathbb{C}_{\mathrm{N}}(V,T,q)$

(iv) Joint inversion of all the experimental data to refine the initial fit parameters.

The initial piece-wise refinement was required to avoid the fitting procedure entering local minima.

4.3.1 Fitting of the $\mathcal{G}(P,T)$ equation of state

In the first step of the inversion, data from four papers were used: $V(P)$ data from Andrault et al. (2003), $V(P)$ and $K_{\mathrm{NR}}(P)$ data from Zhang et al. (2021b), $V(T)$ data from Ito et al. (1974), and the transition pressure at 3000 K (taken to be 90 $\pm$ 1 GPa) from Fischer et al. (2018). Volumes from Fischer et al. (2018) were not used directly, as they involved significantly more scatter than the other datasets.

Some processing of the data was required during fitting to ensure self-consistency. Firstly, because $1/K_{\mathrm{NR}} = -(\partial(\ln V)/\partial P)_N$, volume data from XRD and elastic data from Brillouin and impulsive stimulated light scattering (Zhang et al., 2021b) can be combined to provide independent constraints on the pressure (Kurnosov et al., 2017). To ensure consistency with the reported pressures, hyper-parameters were included in the inversion such that the actual pressure for each dataset was given by:

$$P_{\mathrm{model}} = P_{\mathrm{calibrant}}(a + bP_{\mathrm{calibrant}}) \tag{62}$$

The final values of these hyperparameters after the joint inversion (Section 4.3.4) were $a = 0.9302$, $b = -4.5424 \cdot 10^{-13}$ Pa^{-1} for the Zhang et al. (2021b) data, and $a = 0.9935$, $b = -9.2041 \cdot 10^{-13}$ Pa^{-1} for the Andrault et al. (2003) data.

Given the very small uncertainties in the reported volumes, the model was interrogated to obtain pressures at the experimentally observed volume and temperature. Pressure uncertainties were chosen to be equal to either the reported uncertainty, or $10^8 + 0.01 \cdot P_{\mathrm{calibrant}}$, whichever was the bigger. This downweighted data points with unusually small uncertainties on pressure.

Secondly, the room temperature volume of stishovite in the 1 bar study of Ito et al. (1974) was significantly larger than in the studies of Zhang et al. (2021b) and Andrault et al. (2003). Therefore, all the volumes in that study were scaled by a factor $f = V_{0,\,\mathrm{model}}/V_{0,\,\mathrm{Ito}}$, so that the data could still be used to provide an estimate of $(\partial V/\partial T)_P$. Weighted misfits were obtained using the volume uncertainties from the original paper.

The parameters fit during this stage are given in all but the last two rows of Table 3. The resulting volumes are shown in Figure 3.

4.3.2 Initial fitting of the unit cell properties $\boldsymbol{M}(V,T,q)$

After the initial fitting of the volume and Reuss bulk modulus data, the a, b and c axis lengths were fit using the stishovite and post-stishovite data from Zhang et al. (2021b) and post-stishovite data

	$Q = 0$	$Q = 1$
$\mathcal{F}_0$	-8.174916e+05	-8.121660e+05
V_0	1.401172e-05	1.392651e-05
K_0	3.030507e+11	3.030507e+11
K_0'	4.031062e+00	4.031062e+00
Debye T_0	1.092170e+03	1.109799e+03
γ_0	1.340266e+00	1.340266e+00
q_0	2.122000e+00	2.122000e+00
a_0	-	2.728300e-02
b_0	-	2.857203e-02

Table 3. Properties of stishovite and post-stishovite as constant structural state as obtained from the available data. All properties are given as SI units (J/mol, m^3/mol, Pa, K, $m/mol^{\frac{1}{3}}$)

from Andrault et al. (2003). Data were fit as a function of pressure, using the modified pressures from Section 4.3.1. The uncertainties in the axis lengths were taken to be equal to either the reported uncertainty, or 0.05% of the value of the axis length. As with the modification to the pressure uncertainties in Section 4.3.1, this downweighted data with unusually small uncertainties.

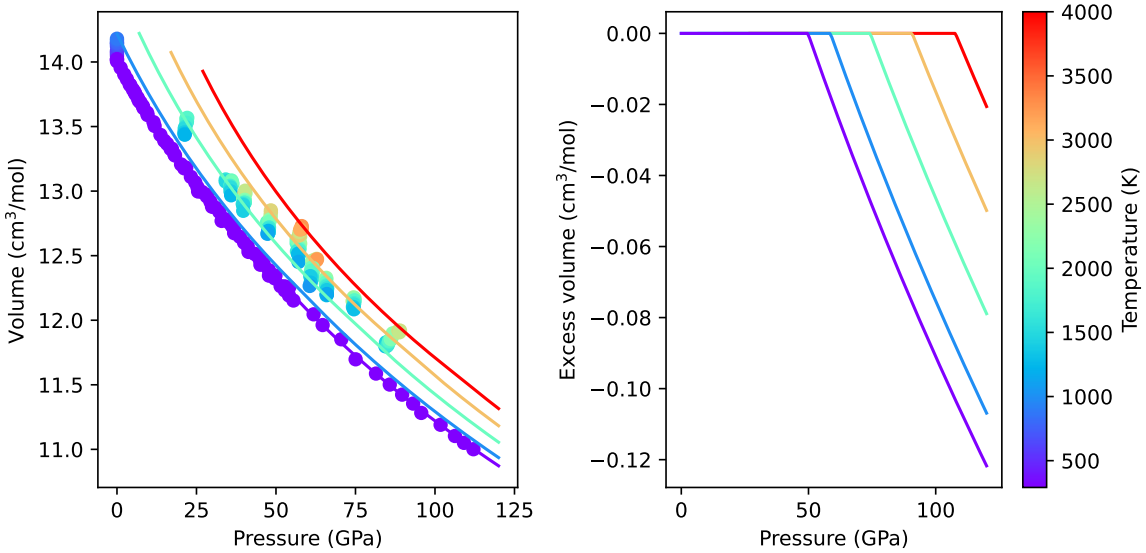

Figure 3. Modelled volume of stishovite-post stishovite as a function of pressure and temperature. Data points are from the published literature (Ito et al., 1974; Andrault et al., 2003; Fischer et al., 2018; Zhang et al., 2021b). The pressures of the data from Andrault et al. (2003) and Zhang et al. (2021b) are adjusted as described in Section 4.3. Data from Fischer et al. (2018) was not used in the inversion, but is shown for comparison with the model.

	a	b_1	c_1	b_2	c_2
Ψ_1	3.947517e-01	3.011252e-01	1.112234e+00	-4.100808e-05	-1.046897e+01
Ψ_2	as above	as above	as above	as above	as above
Ψ_3	(2.104966e-01)	(-6.022504e-01)	as above	(8.201616e-05)	as above
Ψ_{11}	3.213067e-01	9.296219e-01	as above	-1.218009e-02	as above
Ψ_{22}	8.342128e-01	as above	as above	as above	as above
Ψ_{33}	4.930226e-01	-1.467823e-02	as above	-4.592044e-03	as above
Ψ_{44}	1.120120e+00	-2.575796e+00	9.746291e-01	-	-
Ψ_{55}	1.209577e+00	as above	as above	-	-
Ψ_{66}	9.493643e-01	-8.618729e-01	9.980290e-01	-	-

Table 4. Anisotropic parameters for post-stishovite ($Q = 1$). The first three rows correspond to the sum $\Psi_i = \Psi_{i1} + \Psi_{i2} + \Psi_{i3}$. Values in brackets ($\Psi_3$) are not independent - they are uniquely determined by Ψ_1 and Ψ_2.

Available data from Ito et al. (1974) and Fischer et al. (2018) suggests that temperature plays a negligible role in the relative lengths of the a, b and c axes; volume and the structural parameter q have the dominant effect. Furthermore, q appears to have a negligible role in determining the length of the c axis, with all data lying on a single line in V-c space (Figure 4). The values fit during this stage of the inversion are given in the last two rows of Table 3 and the first three rows of Table 4. The resulting evolution of the a, b and c axes is shown in Figure 5.

4.3.3 Initial fitting of the relaxed elastic moduli $\mathbb{C}_N(V, T, q)$

The final data used in the fitting are the elastic moduli from (Zhang et al., 2021b). As for the volume and cell length data, pressures were modified using the hyperparameter values in Section 4.3.1.

Initial attempts at inverting the elasticity data failed to converge on a good solution. The reason for this is that the isentropic compressibility of the three cell axes must be consistent with the corresponding components of the compliance tensor:

$$\beta_{\mathrm{N}i} = \mathbb{S}_{\mathrm{N}i1} + \mathbb{S}_{\mathrm{N}i2} + \mathbb{S}_{\mathrm{N}i3} \tag{63}$$

which are found by inverting the elastic stiffness tensor $\mathbb{S}_{\mathrm{N}} = \mathbb{C}_{\mathrm{N}}^{-1}$. The elastic data from Zhang et al. (2021b) indicated a slightly smaller compressibility along the c axis than the unit cell data used in Section 4.3.2. Making the assumption that the Poisson's ratios are less well constrained than the

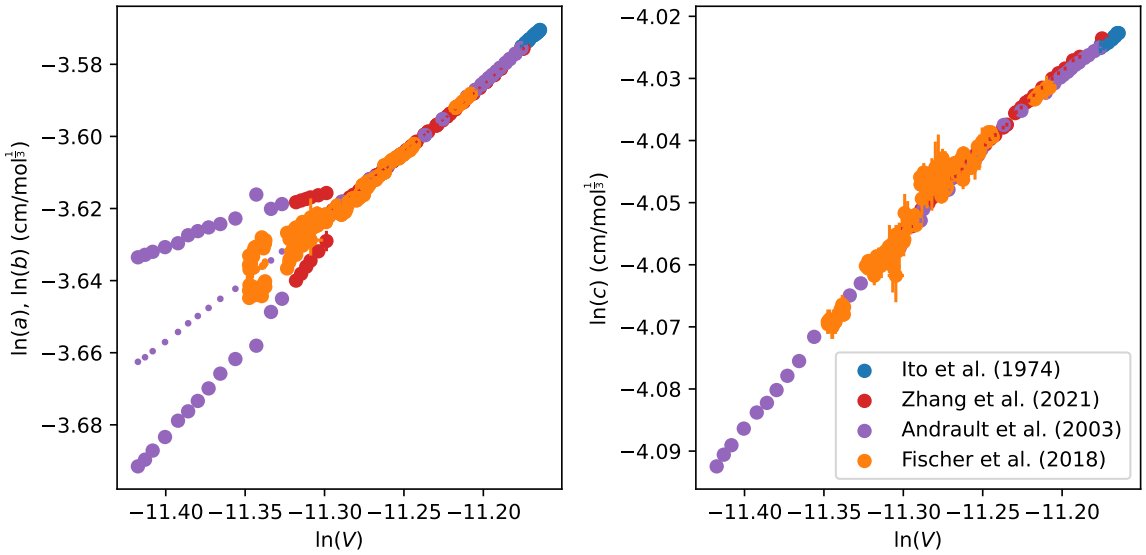

Figure 4. Observed natural logarithm of the a, b and c axis lengths as a function of the natural logarithm of the volume. Data taken from the published literature (Ito et al., 1974; Andrault et al., 2003; Fischer et al., 2018; Zhang et al., 2021b). The pressures of the data from Andrault et al. (2003) and Zhang et al. (2021b), and volumes of Ito et al. (1974) are adjusted as described in Section 4.3. Error bars in both x and y are shown, but are mostly smaller than the data points.

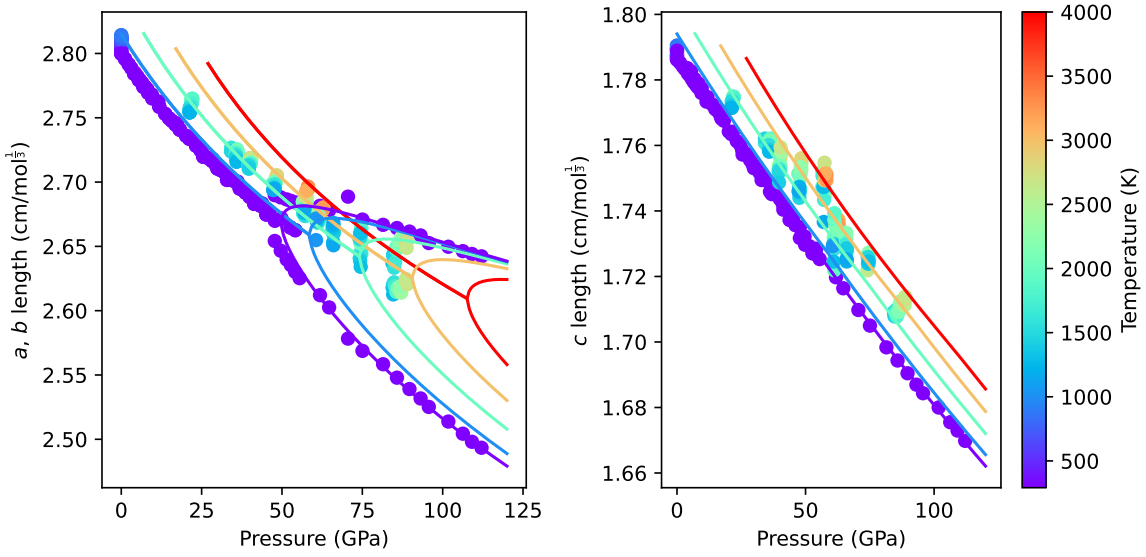

Figure 5. Modelled a, b and c-axis lengths of stishovite-post stishovite as a function of pressure and temperature. Data points are from the published literature (Ito et al., 1974; Andrault et al., 2003; Fischer et al., 2018; Zhang et al., 2021b). The pressures of the data from Andrault et al. (2003) and Zhang et al. (2021b) are adjusted as described in Section 4.3.

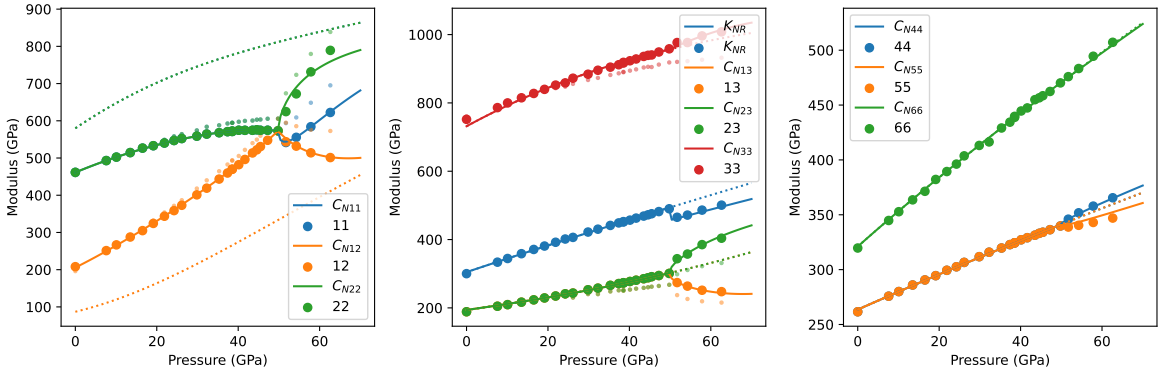

Figure 6. Isentropic elastic stiffness moduli for stishovite and post-stishovite at 298.15 K. Solid lines are the relaxed moduli at the equilibrium value of Q. Dotted lines correspond to the unrelaxed moduli at $Q = 0$. Small dots are the data from (Zhang et al., 2021b) and large dots correspond to the same moduli adjusted to satisfy the unit cell constraints from the same paper.

Young's moduli, I modified only the off-diagonals of the observed elastic compliance matrix:

$$\mathbb{S}_{\mathrm{N,modified12}} = (\mathbb{S}_{\mathrm{N12}} + (\Delta\beta_{\mathrm{N1}} + \Delta\beta_{\mathrm{N2}} - \Delta\beta_{\mathrm{N3}}/2) \tag{64}$$

$$\mathbb{S}_{\mathrm{N,modified13}} = (\mathbb{S}_{\mathrm{N13}} + (\Delta\beta_{\mathrm{N1}} + \Delta\beta_{\mathrm{N3}} - \Delta\beta_{\mathrm{N2}}/2) \tag{65}$$

$$\mathbb{S}_{\mathrm{N,modified23}} = (\mathbb{S}_{\mathrm{N23}} + (\Delta\beta_{\mathrm{N2}} + \Delta\beta_{\mathrm{N3}} - \Delta\beta_{\mathrm{N1}}/2) \tag{66}$$

$$\Delta\beta_{\mathrm{N}i} = \beta_{\mathrm{N,model}i} - \beta_{\mathrm{N,obs}i} \tag{67}$$

These modified values were then used to calculate a modified stiffness tensor. The difference between the original moduli and the modified moduli is shown in Figure 6 (small datapoints are the original data, and larger datapoints are the modified data). It is noteworthy that the data at low pressure is essentially unmodified, with the modification required to match the unit cell data growing with increasing volume.

The misfit was calculated from the difference between this modified stiffness tensor and the model values, weighted by the original uncertainties in the stiffness tensor reported by Zhang et al. (2021b). The values fit during this stage of the inversion are given in the last six rows of Table 4. The resulting elastic stiffness tensor at 298.15 K is shown in Figure 6.

4.3.4 Final joint inversion and model properties

After obtaining an initial set of parameters from the previous steps, all the parameters were simultaneously refit using all the experimental data to obtain a global minimum misfit, producing the reported figures in Tables 3 and 4 and in the text (for the hyperparameters).

Once created, the model can be interrogated for any elastic properties at any pressure and tem-

perature. Bearing in mind that no high-pressure - high-temperature data was used apart from a single transition pressure from (Fischer et al., 2018), the data is in reasonable agreement with the available cell data from Fischer et al. (2018) (Figure 5).

The modelled elastic moduli in Figure 6 are also in very good agreement with the data modified from (Zhang et al., 2021b), suggesting that the formulation of the anisotropic properties contained sufficient free parameters to match the experimental data without noticeable over-fitting.

Seismic velocities, linear compressibilities and extrema in Poisson's ratios are provided just below (Figure 7) and above (Figure 8) the stishovite-post-stishovite transition. As expected, V_{S2} velocities approach zero along the $[1, 1, 0]$ direction from both sides of the transition. Also as expected, the linear compressibility is positive in all directions below the transition - i.e. squeezing stishovite uniaxially results in a smaller volume. In contrast, above the transition, linear compressibility along the longer axis is negative - squeezing the structure uniaxially results in volume expansion. This negative compressibility persists until about 10 GPa above the transition.

Another interesting observation from the model is that near the transition, the minimum Poisson ratio in almost every direction is negative; that is, when stretched along any direction, crystals of stishovite and post-stishovite get longer in an orthogonal direction. As can be seen in Figures 7) and 8. This auxetic behaviour decreases in intensity away from the transition. It also becomes more restricted away from the transition - there are almost no directions of auxeticity 40 GPa below the transition, and auxeticity more than 10 GPa above the transition is restricted to a broad, persistent band surrounding the plane perpendicular to the b axis. A pressure profile extending Figures 7) and 8 are provided as Supplementary Materials.

Finally, Figure 9 shows the isotropic V_P, V_Φ and V_S velocities calculated from the Reuss, Voigt and Voigt-Reuss-Hill (VRH) isentropic bulk and shear moduli. Note the small discontinuity in the VRH compressional and bulk sound velocities at the transition that results from the discontinuous change in the Reuss bulk modulus. The reduction in V_S associated with the transition has previously been connected with the observation of seismic scatterers in the lower mantle (Kaneshima & Helffrich, 1999; Niu, 2014; Kaneshima, 2019).

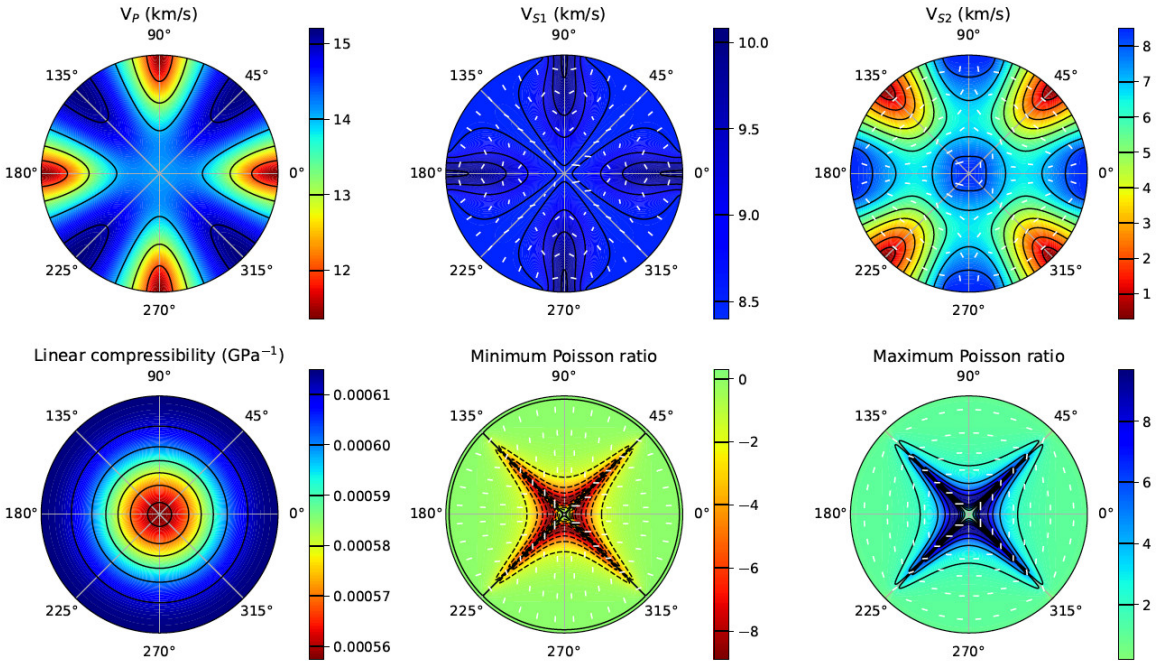

Figure 7. Modelled elastic properties at 77.43 GPa, 2200 K, which is 0.1 GPa lower pressure than the stishovite-post-stishovite transition. Upper hemisphere projection. S-wave velocities are plotted with white lines corresponding to the directions of particle motion. Minimum and maximum Poisson ratios are plotted at positions on the focal sphere that correspond to the axial propagation direction, with white lines corresponding to the lateral directions.

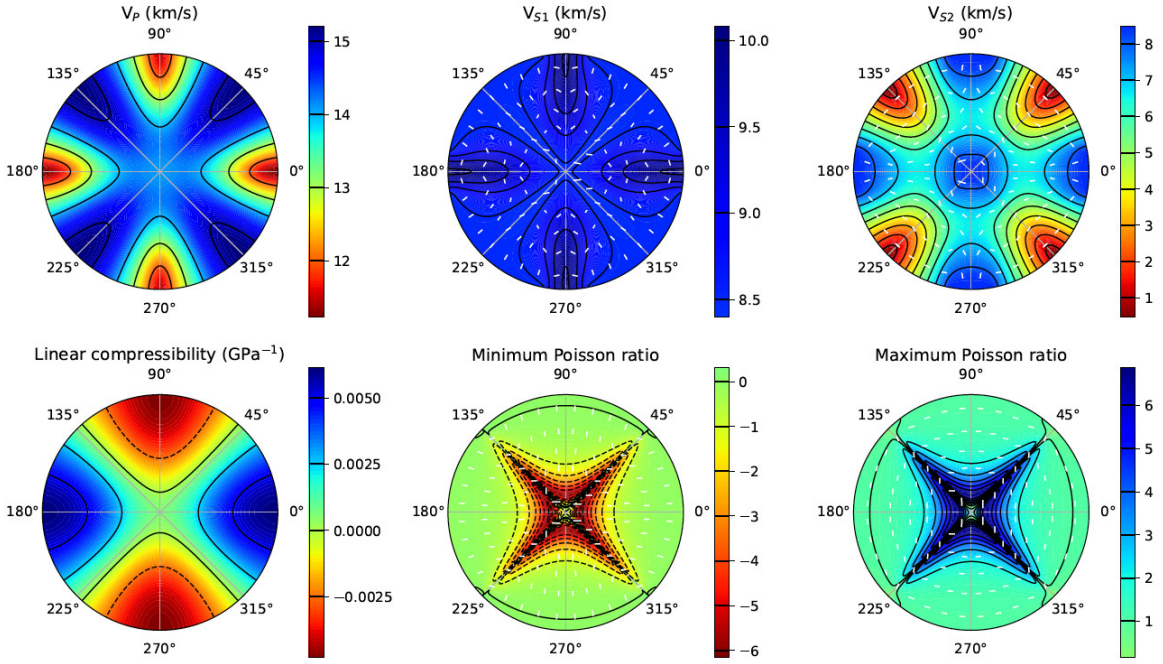

Figure 8. Modelled elastic properties at 77.63 GPa, 2200 K, which is 0.1 GPa higher pressure than the stishovite-post-stishovite transition. Most material properties are similar to Figure 7, with the exception of the linear compressibility. Upper hemisphere projection. S-wave velocities are plotted with white lines corresponding to the directions of particle motion. Minimum and maximum Poisson ratios are plotted at positions on the focal sphere that correspond to the axial propagation direction, with white lines corresponding to the lateral directions.

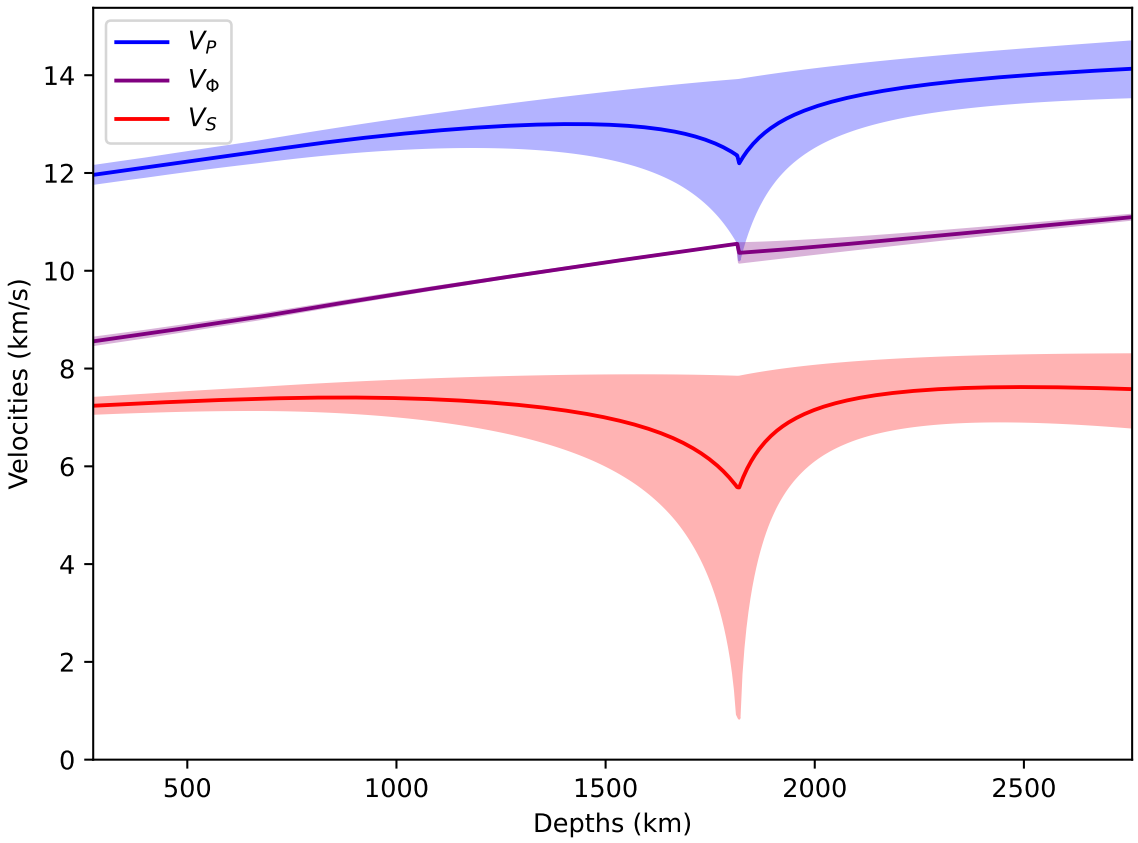

Figure 9. Isotropic seismic velocities of stishovite-post-stishovite along a mantle geotherm (Brown & Shankland, 1981). Shaded regions are bounded by the Reuss and Voigt estimates, solid line represents the Voigt-Reuss-Hill average.

5 DISCUSSION

5.1 Thermodynamics versus atom-scale behaviour

The model proposed here is purely thermodynamic: all the properties investigated here are macroscopic properties that are functions of thermodynamic energy derivatives. The derivations of unrelaxed, relaxed and time-dependent properties in Section 3 are entirely general; if one can find an appropriate form for the Gibbs energy as a function of P, T, composition $\boldsymbol{x}$ and appropriate isochemical degrees of freedom $\boldsymbol{q}$, and a description of the anisotropic tensor Ψ as a function of V, T, $\boldsymbol{x}$ and $\boldsymbol{q}$, all thermodynamic and elastic properties can be determined at arbitrary state.

The thermodynamic model, however, says nothing about the atom-scale behaviour of the materials studied. This atomic behaviour determines how many isochemical variables $\boldsymbol{q}$ are required to describe the observed behaviour, and the shape of the $\mathcal{G}(P,T,\boldsymbol{x},\boldsymbol{q})$ and $\Psi(V,T,\boldsymbol{x},\boldsymbol{q})$ functions. This atom-scale behaviour can be probed by diffraction or spectroscopic techniques.

In the case of stishovite, one structural parameter Q appears to be sufficient to describe the cell and elastic properties over large regions of P-T space. This parameter Q can be associated with tilting of SiO_6 octahedra (Zhang et al., 2023, Figure 2) and directly related values like oxygen positions (Criniti et al., 2023). The stishovite-post-stishovite transition is associated with a sharp minimum in the frequency of rotational vibration of O atoms about the c-axis. In the jargon of spectroscopists, this is known as "softening" of the "B_{1g}" optical phonon mode (with the symmetry of the "Γ_3^+ irreducible representation", in stishovite) or "A_g" mode (in post-stishovite) (Kingma et al., 1995), which can be observed using Raman spectroscopy (Kingma et al., 1995). Splitting of vibrations of pairs of oxygen atoms linked through a silicon atom along [110] or [-110] is also observed. The vibration of these atoms is out-of-phase and colinear with the c-axis. The spectroscopic jargon is splitting of the "E_g" optical phonon mode (with the symmetry of the "Γ_5^- irreducible representation") into "B_{2g}" and "B_{3g}" modes (Kingma et al., 1995). "Optical phonon" just means out of phase atomic motions, where the word optical arises because the opposed displacement creates an electrical polarization that interacts with electromagnetic fields, and can therefore be excited by infrared radiation. Useful diagrams illustrating the modes in the stishovite structure (isostructural with rutile) and mode and symmetry naming conventions are given by Traylor et al. (1971).

5.2 Spontaneity, coupling, and the "properness" of ferroic phase transitions

So-called "ferroic" phase transitions are those which involve large "spontaneous" changes in physical properties over small changes in state. In ferroelastic transitions such as the stishovite-post stishovite transition, a change in stress induces a change in strain; in ferroelectrics, a change in electric field

strength induce an electric displacement; and in ferromagnets, a change in magnetic field strength induce a change in magnetic flux density. However, transitions need not only involve energy conjugates (stress-strain, electric field strength-displacement, etc.); temperature, stress, electric and magnetic fields can all potentially induce large changes in entropy, strain, electric displacement and magnetic flux density. For discussion of some of the cross terms and associated second derivatives, see (Nye et al., 1985, Chapter 10).

Classically, ferroic transitions have been subdivided into three groups based on how the "spontaneous" change in a property "y", such as excess entropy, or strain, is modelled (Wadhawan, 1982; Carpenter, 2006):

- Proper: where y can be used directly as q:

$$\mathcal{F}(V,T,q,y) = \mathcal{F}_0(V,T) + a(V,T)y^2 + by^4 + \dots \tag{68}$$

- Pseudoproper: y cannot be used as the order parameter, but is (bilinearly) coupled to it (Dvořák, 1974). The order parameter and property with "spontaneous" changes must have the same symmetries.

$$\mathcal{F}(V,T,q,y) = \mathcal{F}_0(V,T) + a(V,T)q^2 + bq^4 + \dots + fqy \tag{69}$$

- Improper: where there are multiple order parameters that together have a different symmetry to that of y:

$$\mathcal{F}(V,T,q,y) = \mathcal{F}_0(V,T) + A_{ij}(V,T)q_iq_j + B_{ijkl}q_iq_jq_kq_l + \dots + f_{ij}q_iq_jy \tag{70}$$

where the A_{ij}, B_{ijkl} etc. satisfy the symmetry of the phase.

This study demonstrates that a self-consistent Landau model can be designed that does not include "y" (the property with "spontaneous" changes) as an independent variable in the energy function. Instead, both the energy to be minimised and y are written as a function of the natural variables (e.g. Equation 6):

$$\mathcal{F} = \mathcal{F}(V,T,q),\ y = y(V,T,q)$$

As a consequence, when using the Landau model proposed in this study, the terms proper, pseudoproper and improper are not particularly insightful. The equivalent mathematical property of interest is whether each component of y varies approximately linearly with q.

5.3 Extensions to electric and magnetic behaviour

Although it is beyond the scope of this study, it is worth considering how the formalism might be extended to include electric and magnetic properties. The Helmholtz energy of Equation 5 would need to be extended to include the electric field strength $\boldsymbol{e}$ [V/m] and magnetic field strength $\boldsymbol{h}$ [A/m]

as independent variables, with the electric displacement $\boldsymbol{d}$ [C/m^2] and magnetic flux density $\boldsymbol{b}$ [T] additional properties in the Legendre transformation from the internal energy:

$$\mathcal{F} = \mathcal{F}(V, T, \boldsymbol{e}, \boldsymbol{h}, \boldsymbol{n}, \bar{\varepsilon}) = \mathcal{E} - TS - \boldsymbol{d}\boldsymbol{e} - \boldsymbol{b}\boldsymbol{h} \tag{71}$$

The z vector would have to be extended to include these parameters ($\boldsymbol{z} = \{\boldsymbol{\varepsilon}, T, \boldsymbol{e}, \boldsymbol{h}\}$). The additional first derivatives of the Helmholtz energy would be:

$$-V\boldsymbol{d} = \frac{\partial \mathcal{F}}{\partial \boldsymbol{e}} \tag{72}$$

$$-V\boldsymbol{b} = \frac{\partial \mathcal{F}}{\partial \boldsymbol{h}} \tag{73}$$

The second derivatives would form an extended block tensor:

$$\frac{\partial^2 \mathcal{F}}{\partial z \partial z} = \left[\begin{array}{c|c|c|c} V\frac{\partial \boldsymbol{\sigma}}{\partial \boldsymbol{\varepsilon}} & V\frac{\partial \boldsymbol{\sigma}}{\partial T} & V\frac{\partial \boldsymbol{\sigma}}{\partial \boldsymbol{e}} & V\frac{\partial \boldsymbol{\sigma}}{\partial \boldsymbol{h}} \\ \hline -\frac{\partial N}{\partial \boldsymbol{\varepsilon}} & -\frac{\partial N}{\partial T} & -\frac{\partial N}{\partial \boldsymbol{e}} & -\frac{\partial N}{\partial \boldsymbol{h}} \\ \hline -V\frac{\partial \boldsymbol{d}}{\partial \boldsymbol{\varepsilon}} & -V\frac{\partial \boldsymbol{d}}{\partial T} & -V\frac{\partial \boldsymbol{d}}{\partial \boldsymbol{e}} & -V\frac{\partial \boldsymbol{d}}{\partial \boldsymbol{h}} \\ \hline -V\frac{\partial \boldsymbol{b}}{\partial \boldsymbol{\varepsilon}} & -V\frac{\partial \boldsymbol{b}}{\partial T} & -V\frac{\partial \boldsymbol{b}}{\partial \boldsymbol{e}} & -V\frac{\partial \boldsymbol{b}}{\partial \boldsymbol{h}} \end{array}\right] = \left[\begin{array}{c|c|c|c} V\mathbb{C}_{\mathrm{T}} & V\boldsymbol{\pi} & -V\boldsymbol{D} & -V\boldsymbol{\Lambda} \\ \hline V\boldsymbol{\pi}^{\mathrm{T}} & -c_{\boldsymbol{\varepsilon}}/T & -V\boldsymbol{p} & -V\boldsymbol{\phi} \\ \hline -V\boldsymbol{D} & -V\boldsymbol{p} & -V\boldsymbol{\epsilon} & -V\boldsymbol{A} \\ \hline -V\boldsymbol{\Lambda} & -V\boldsymbol{\phi} & -V\boldsymbol{A} & -V\boldsymbol{\mu} \end{array}\right] \tag{74}$$

where the elements of the tensor are (Nye et al., 1985; Fuentes-Cobas et al., 2011):

- $\boldsymbol{D}$: the piezoelectric tensor
- $\boldsymbol{p}$: the pyroelectric tensor
- $\boldsymbol{\epsilon}$: the absolute dielectric permittivity
- $\boldsymbol{A}$: the magnetoelectric tensor
- $\boldsymbol{\Lambda}$: the piezomagnetic tensor
- $\boldsymbol{\phi}$: the pyromagnetic tensor
- $\boldsymbol{\mu}$: the magnetic permeability

The chain rule is required to obtain $\boldsymbol{D}$ and $\boldsymbol{\Lambda}$ from the expression for the Helmholtz energy (Appendix B):

$$D_{ijk} = \frac{\partial d_i}{\partial \varepsilon_{jk}} = (\delta_{jk} V)\frac{\partial d_i}{\partial V} + \left(\delta_{lj}\delta_{mk} - \frac{\beta_{\mathrm{T}lm}}{\beta_{\mathrm{RT}}}\delta_{jk}\right)\frac{\partial d_i}{\partial \bar{\varepsilon}_{lm}} \tag{75}$$

$$\Lambda_{ijk} = \frac{\partial b_i}{\partial \varepsilon_{jk}} = (\delta_{jk} V)\frac{\partial b_i}{\partial V} + \left(\delta_{lj}\delta_{mk} - \frac{\beta_{\mathrm{T}lm}}{\beta_{\mathrm{RT}}}\delta_{jk}\right)\frac{\partial b_i}{\partial \bar{\varepsilon}_{lm}} \tag{76}$$

The non-zero elements for phases of different symmetry types are provided by Litvin & Janovec (2014).

6 BENEFITS OF THE NEW FORMULATION

The Landau formulation for isochemical flexibility in anisotropic phases proposed in this study has the following benefits:

- It is fully self-consistent.
- The underlying Landau energy minimization is applied only to the scalar $\mathcal{G}(P, T, \boldsymbol{x}, \boldsymbol{q})$ equation of state, rather than to the entire anisotropic model. As a result, Gibbs minimisation is performed only over the structural parameters $\boldsymbol{q}$ at any given P-T condition, rather than $\boldsymbol{q}$ and the spontaneous strains or polarisations.
- It is easily extended to accommodate additional degrees of compositional or isochemical freedom. Phases requiring more than one parameter $\boldsymbol{q}$ include quartz, where static and dynamic tilts both affect the Gibbs energy and elastic properties of the phase (Wells et al., 2002; Antao, 2016; Angel et al., 2017), or troilite, which experiences spin and structural transitions that intersect (Urakawa et al., 2004).

ACKNOWLEDGMENTS

Paul Asimow introduced me to seismic relaxation many years ago at the 2014 CIDER workshop. Thanks to him, all the participants, and NSF for providing such a fantastic environment for learning.

This work was supported by NERC Large Grant MC-squared (Award No. NE/T012633/1) and STFC (Grant No. ST/R001332/1). Any mistakes or oversights are my own.

DATA AVAILABILITY

The anisotropic equation of state described in this paper is provided as a contribution to the BurnMan open source software project: `https://github.com/geodynamics/burnman` (Cottaar et al., 2014; Myhill et al., 2023).

References

Andrault, D., Angel, R. J., Mosenfelder, J. L., & Le Bihan, T., 2003. Equation of state of stishovite to lower mantle pressures, *American Mineralogist*, **88**(2-3), 301–307.

Angel, R. J., Alvaro, M., Miletich, R., & Nestola, F., 2017. A simple and generalised p–t–v eos for continuous phase transitions, implemented in eosfit and applied to quartz, *Contributions to Mineralogy and Petrology*, **172**(5).

Antao, S. M., 2016. Quartz: structural and thermodynamic analyses across the α-β transition with origin of negative thermal expansion (nte) in β quartz and calcite, *Acta Crystallographica Section B: Structural Science, Crystal Engineering and Materials*, **72**(2), 249–262.

Brown, J. M. & Shankland, T. J., 1981. Thermodynamic parameters in the Earth as determined from seismic profiles, *Geophysical Journal International*, **66**(3), 579–596.

Buchen, J., 2021. *Seismic Wave Velocities in Earth's Mantle from Mineral Elasticity*, chap. 3, pp. 51–95, American Geophysical Union (AGU).

Buchen, J., Marquardt, H., Schulze, K., Speziale, S., Tiziana, Nishiyama, N., & Hanfland, M., 2018. Equation of state of polycrystalline stishovite across the tetragonal-orthorhombic phase transition, *Journal of Geophysical Research: Solid Earth*, **123**(9), 7347–7360.

Cámara, F., Oberti, R., Iezzi, G., & Ventura, G. D., 2003. The p21/m ¡-¿ c2/m phase transition in synthetic amphibole na namg mg_5 si_8 o_{22} $(oh)_2$: thermodynamic and crystal-chemical evaluation, *Physics and Chemistry of Minerals*, **30**(9), 570–581.

Carpenter, M. A., 2006. Elastic properties of minerals and the influence of phase transitions, *American mineralogist*, **91**(2-3), 229–246.

Carpenter, M. A. & Salje, E. K., 1998. Elastic anomalies in minerals due to structural phase transitions, *European Journal of Mineralogy*, pp. 693–812.

Carpenter, M. A., Salje, E. K., Graeme-Barber, A., Wruck, B., Dove, M. T., & Knight, K. S., 1998. Calibration of excess thermodynamic properties and elastic constant variations associated with the alpha¡−¿ beta phase transition in quartz, *American mineralogist*, **83**(1-2), 2–22.

Carpenter, M. A., Hemley, R. J., & Mao, H.-k., 2000. High-pressure elasticity of stishovite and the p42/mnm–pnnm phase transition, *Journal of Geophysical Research: Solid Earth*, **105**(B5), 10807–10816.

Coddington, E. A. & Levinson, N., 1984. *Theory of ordinary differential equations*, Tata McGraw-Hill Education, 9th edn.

Cottaar, S., Heister, T., Rose, I., & Unterborn, C., 2014. Burnman: A lower mantle mineral physics toolkit, *Geochemistry, Geophysics, Geosystems*, **15**(4), 1164–1179.

Criniti, G., Ishii, T., Kurnosov, A., Glazyrin, K., & Ballaran, T. B., 2023. High-pressure phase transition and equation of state of hydrous al-bearing silica, *American Mineralogist*, **108**(8), 1558–1568.

Davies, G. F., 1974. Effective elastic moduli under hydrostatic stress – I. quasi-harmonic theory, *Journal of Physics and Chemistry of Solids*, **35**, 1513–1520.

Devonshire, A., 1949. Xcvi. theory of barium titanate, *The London, Edinburgh, and Dublin Philosophical Magazine and Journal of Science*, **40**(309), 1040–1063.

Dove, M. T., 1997. Theory of displacive phase transitions in minerals, *American Mineralogist*, **82**(3-4), 213–244.

Dvořák, V., 1974. Improper ferroelectrics, *Ferroelectrics*, **7**(1), 1–9.

Fischer, R., Campbell, A., Chidester, B., Reaman, D., Thompson, E. C., Pigott, J., Prakapenka, V., & Smith, J., 2018. Equations of state and phase boundary for stishovite and cacl2-type sio2, *American Mineralogist*, **103**, 792–802.

Fuentes-Cobas, L., Matutes-Aquino, J., & Fuentes-Montero, M., 2011. Chapter three - magnetoelectricity, in *Handbook of Magnetic Materials*, vol. 19, pp. 129–229, ed. Buschow, K., Elsevier.

Ganguly, J., 1982. Mg-fe order-disorder in ferromagnesian silicates: Ii. thermodynamics, kinetics, and geological applications., *Journal of Environmental Sciences (China) English Ed*, pp. 58–99.

Grønvold, F. & Stølen, S., 1992. Thermodynamics of iron sulfides ii. heat capacity and thermodynamic properties of fes and of fe0.875s at temperatures from 298.15 k to 1000 k, of fe0.98s from 298.15 k to 800 k, and of fe0.89s from 298.15 k to about 650 k. thermodynamics of formation, *The Journal of Chemical Thermodynamics*, **24**(9), 913–936.

Heinemann, S., Sharp, T. G., Seifert, F., & Rubie, D. C., 1997. The cubic-tetragonal phase transition in the system majorite (mg 4 si 4 o 12) - pyrope (mg 3 al 2 si 3 o 12), and garnet symmetry in the earth's transition zone, *Physics and Chemistry of Minerals*, **24**(3), 206–221.

Helgeson, H. C., 1978. Summary and critique of the thermodynamic properties of rock-forming minerals, *American Journal of Science*, **278**, 1–229.

Hirose, K. & Fei, Y., 2002. Subsolidus and melting phase relations of basaltic composition in the uppermostlower mantle, *Geochimica et Cosmochimica Acta*, **66**(12), 2099–2108.

Holland, T. J. B., Hudson, N. F. C., Powell, R., & Harte, B., 2013. New Thermodynamic Models and Calculated Phase Equilibria in NCFMAS for Basic and Ultrabasic Compositions through the Transition Zone into the Uppermost Lower Mantle, *Journal of Petrology*, **54**, 1901–1920.

Holzapfel, G., 2000. *Nonlinear Solid Mechanics: A Continuum Approach for Engineering*, John Wiley and Sons, Ltd.

Ito, H., Kawada, K., & Akimoto, S.-i., 1974. Thermal expansion of stishovite, *Physics of the Earth and Planetary Interiors*, **8**(3), 277–281.

Kaneshima, S., 2019. Seismic scatterers in the lower mantle near subduction zones, *Geophysical Journal International*, **219**(Supplement_1), S2–S20.

Kaneshima, S. & Helffrich, G., 1999. Dipping low-velocity layer in the mid-lower mantle: evidence for geochemical heterogeneity, *Science*, **283**(5409), 1888–1892.

Kimizuka, H., Kaburaki, H., & Kogure, Y., 2003. Molecular-dynamics study of the high-temperature elasticity of quartz above the α-β phase transition, *Physical Review B*, **67**(2), 024105.

Kingma, K. J., Cohen, R. E., Hemley, R. J., & Mao, H.-k., 1995. Transformation of stishovite to a denser phase at lower-mantle pressures, *Nature*, **374**(6519), 243–245.

Kityk, A. V., Schranz, W., Sondergeld, P., Havlik, D., Salje, E. K. H., & Scott, J. F., 2000. Low-frequency superelasticity and nonlinear elastic behavior ofsrtio3, *Physical Review B*, **61**(2), 946–956.

Kurnosov, A., Marquardt, H., Frost, D. J., Ballaran, T. B., & Ziberna, L., 2017. Evidence for a Fe^{3+}-rich pyrolitic lower mantle from (Al,Fe)-bearing bridgmanite elasticity data, *Nature*, **543**, 543–546.

Lacivita, V., D'arco, P., Mustapha, S., Bernardes, D. F., Dovesi, R., Erba, A., & Rérat, M., 2020. Ab initio compressibility of metastable low albite: revealing a lambda-type singularity at pressures of the Earth's upper mantle, *Physics and Chemistry of Minerals*, **47**(10), 1–13.

Lakshtanov, D. L., Sinogeikin, S. V., & Bass, J. D., 2007. High-temperature phase transitions and elasticity of silica polymorphs, *Physics and Chemistry of Minerals*, **34**(1), 11–22.

Landau, L., 1935. Zur theorie der anomalien der spezifischen warme, *Phys. Z. Sowjet*, **8**, 113.

Landau, L., 1937a. Zur theorie der phasenum-wandlungen i, *Phys. Z. Sowjet*, **11**, 26.

Landau, L., 1937b. Zur theorie der phasenum-wandlungen ii, *Phys. Z. Sowjet*, **11**, 545.

Landau, L., 2008. On the Theory of Phase Transitions, *Ukrainian Journal of Physics*, **53**, 25–35.

Landau, L. & Ginzburg, V. L., 1950. On the theory of superconductivity, *JUTP*, **20**, 1064.

Le Chatelier, H., 1890. Sur la dilatation du quartz, *Bulletin de Minéralogie*, **13**(3), 112–118.

Liakos, J. & Saunders, G., 1982. Application of the landau theory to elastic phase transitions, *Philosophical Magazine A*, **46**(2), 217–242.

Litvin, D. B. & Janovec, V., 2014. Spontaneous tensor properties for multiferroic phases, *Ferroelectrics*, **461**(1), 10–15.

Lüthi, B. & Rehwald, W., 1981. Ultrasonic studies near structural phase transitions, in *Structural Phase Transitions I*, pp. 131–184, eds Müller, K. A. & Thomas, H., Springer Berlin Heidelberg, Berlin, Heidelberg.

Mookherjee, M., Mainprice, D., Maheshwari, K., Heinonen, O., Patel, D., & Hariharan, A., 2016. Pressure induced elastic softening in framework aluminosilicate- albite (NaAlSi3O8), *Scientific Reports*, **6**(1), 34815.

Myhill, R., 2024. An anisotropic equation of state for solid solutions (in prep.), *Geophysical Journal International*.

Myhill, R. & Connolly, J. A., 2021. Notes on the creation and manipulation of solid solution models, *Contributions to Mineralogy and Petrology*, **176**(10), 1–19.

Myhill, R., Cottaar, S., Heister, T., Rose, I., Unterborn, C., Dannberg, J., & Gassmoeller, R., 2023. BurnMan – a Python toolkit for planetary geophysics, geochemistry and thermodynamics, *The Journal of Open Source Software*, **8**(87), 5389.

Niu, F., 2014. Distinct compositional thin layers at mid-mantle depths beneath northeast china revealed by the usarray, *Earth and Planetary Science Letters*, **402**, 305–312.

Nye, J. F. et al., 1985. *Physical properties of crystals: their representation by tensors and matrices*, Oxford University Press.

Redfern, S. A., 1998. Time-temperature-dependent m-site ordering in olivines from high-temperature neutron time-of-flight diffraction, *Physica B: Condensed Matter*, **241-243**, 1189–1196, Proceedings of the International Conference on Neutron Scattering.

Redfern, S. A., Harrison, R. J., O'Neill, H. S., & Wood, D. R., 1999. Thermodynamics and kinetics of cation ordering in mgal2o4 spinel up to 1600 °c from in situ neutron diffraction, *American Mineralogist*, **84**(3), 299–310.

Redfern, S. A. T., 2000. Order-Disorder Phase Transitions, *Reviews in Mineralogy and Geochemistry*, **39**(1), 105–133.

Reynard, B., Bass, J. D., & Brenizer, J., 2010. High-temperature elastic softening of orthopyroxene and seismic properties of the lithospheric upper mantle, *Geophysical Journal International*, **181**(1), 557–566.

Salje, E., 1985. Thermodynamics of sodium feldspar i: order parameter treatment and strain induced coupling effects, *Physics and Chemistry of Minerals*, **12**(2), 93–98.

Schranz, W., Tröster, A., Koppensteiner, J., & Miletich, R., 2007. Finite strain landau theory of high pressure phase transformations, *Journal of Physics: Condensed Matter*, **19**(27), 275202.

Seifert, F. A. & Virgo, D., 1975. Kinetics of the fe2+-mg, order-disorder reaction in anthophyllites: Quantitative cooling rates, *Science*, **188**(4193), 1107–1109.

Slonczewski, J. C. & Thomas, H., 1970. Interaction of elastic strain with the structural transition of strontium titanate, *Physical Review B*, **1**(9), 3599–3608.

Stixrude, L. & Lithgow-Bertelloni, C., 2005. Thermodynamics of mantle minerals - I. Physical properties, *Geophysical Journal International*, **162**, 610–632.

Stixrude, L. & Lithgow-Bertelloni, C., 2022. Thermal expansivity, heat capacity and bulk modulus of the mantle, *Geophysical Journal International*, **228**(2), 1119–1149.

Stixrude, L., Lithgow-Bertelloni, C., Kiefer, B., & Fumagalli, P., 2007. Phase stability and shear softening in $casio_3$ perovskite at high pressure, *Physical Review B*, **75**(2), 024108.

Ter Haar, D., 2013. *Collected papers of LD Landau*, Elsevier.

Thompson, A. & Perkins, E., 1981. Lambda transitions in minerals, in *Thermodynamics of minerals and melts*, pp. 35–62, Springer.

Traylor, J. G., Smith, H. G., Nicklow, R. M., & Wilkinson, M. K., 1971. Lattice dynamics of rutile, *Phys. Rev. B*, **3**, 3457–3472.

Tröster, A., Schranz, W., & Miletich, R., 2002. How to couple landau theory to an equation of state, *Phys. Rev. Lett.*, **88**, 055503.

Tröster, A., Schranz, W., Karsai, F., & Blaha, P., 2014. Fully consistent finite-strain landau theory for high-pressure phase transitions, *Physical Review X*, **4**(3).

Tröster, A., Ehsan, S., Belbase, K., Blaha, P., Kreisel, J., & Schranz, W., 2017. Finite-strain landau theory applied to the high-pressure phase transition of lead titanate, *Phys. Rev. B*, **95**, 064111.

Urakawa, S., Someya, K., Terasaki, H., Katsura, T., Yokoshi, S., Funakoshi, K.-i., Utsumi, W., Katayama, Y., Sueda, Y.-i., & Irifune, T., 2004. Phase relationships and equations of state for FeS at high pressures and temperatures and implications for the internal structure of Mars, *Physics of the Earth and Planetary Interiors*, **143**, 469–479.

Wadhawan, V. K., 1982. Ferroelasticity and related properties of crystals, *Phase Transitions*, **3**(1), 3–103.

Welche, P. R. L., Heine, V., & Dove, M. T., 1998. Negative thermal expansion in beta-quartz, *Physics and Chemistry of Minerals*, **26**(1), 63–77.

Wells, S. A., Dove, M. T., Tucker, M. G., & Trachenko, K., 2002. Real-space rigid-unit-mode analysis of dynamic disorder in quartz, cristobalite and amorphous silica, *Journal of Physics: Condensed Matter*, **14**(18), 4645.

Wu, Z., Justo, J. F., & Wentzcovitch, R. M., 2013. Elastic anomalies in a spin-crossover system: Ferropericlase at lower mantle conditions, *Physical Review Letters*, **110**(22).

Yeganeh-Haeri, A., Weidner, D. J., & Parise, J. B., 1992. Elasticity of α-cristobalite: a silicon dioxide with a negative poisson's ratio, *Science*, **257**(5070), 650–652.

Zhang, N. B., Cai, Y., Yao, X. H., Zhou, X. M., Li, Y. Y., Song, C. J., Qin, X. Y., & Luo, S. N., 2018. Spin transition of ferropericlase under shock compression, *AIP Advances*, **8**(7), 075028.

Zhang, Y., Chariton, S., He, J., Fu, S., Prakapenka, V. B., & Lin, J.-F., 2021a. Ferroelastic post-stishovite transition mechanism revealed by single-crystal x-ray diffraction refinements at high pressure, *Earth and Space Science Open Archive*, p. 26.

Zhang, Y., Fu, S., Wang, B., & Lin, J.-F., 2021b. Elasticity of a pseudoproper ferroelastic transition from stishovite to post-stishovite at high pressure, *Phys. Rev. Lett.*, **126**, 025701.

Zhang, Y., Fu, S., Karato, S., Okuchi, T., Chariton, S., Prakapenka, V. B., & Lin, J., 2022. Elasticity of hydrated al-bearing stishovite and post-stishovite: Implications for understanding regional seismic v s anomalies along subducting slabs in the lower ma, *Journal of Geophysical Research: Solid Earth*, **127**(4).

Zhang, Y., Chariton, S., He, J., Fu, S., Xu, F., Prakapenka, V. B., & Lin, J.-F., 2023. Atomistic insight into the ferroelastic post-stishovite transition by high-pressure single-crystal x-ray diffraction, *American Mineralogist*, **108**(1), 110–119.

APPENDIX A: CALCULATING RELAXED THERMODYNAMIC PROPERTIES

Relaxed thermodynamic properties are determined by minimizing an appropriate thermodynamic potential, allowing some or all isochemical structural variables to vary freely. Similar mathematical derivations can be used to quantify the effective isotropic thermodynamics of multiphase assemblages by varying the pressure and temperature (Stixrude & Lithgow-Bertelloni, 2022), or consider the anisotropic properties of a single phase, as we do here.

Let us seek expressions for the relaxed second order derivatives of the Helmholtz energy. We first define a set of functions $P_l(\boldsymbol{M}, T, \boldsymbol{q})$ that describe the partial derivatives of the Helmholtz energy with respect to $\boldsymbol{q}$:

$$P_l(\boldsymbol{M}, T, \boldsymbol{q}) = \frac{\partial \mathcal{F}}{\partial q_l} \tag{A.1}$$

where $\boldsymbol{M}$ is the extensive metric tensor, with elements having units of m, and $\boldsymbol{q}$ are the unitless isochemical structural vectors. The minimization of $\mathcal{F}$ is achieved when

$$P_l(\boldsymbol{M}, T, \boldsymbol{q}^*(\boldsymbol{M}, T)) = 0_l \tag{A.2}$$

The relaxed properties $\mathbb{C}_{\mathrm{T}}^*$, $\boldsymbol{\pi}^*$ and c_ε^* depend on the way in which $\boldsymbol{q}^*$ varies due to small changes in $\boldsymbol{\varepsilon}$ or T (here collected as $\boldsymbol{z} = \{\boldsymbol{\varepsilon}, T\}$). This dependence can be determined by applying the chain rule:

$$\frac{\partial P_l}{\partial z_j} + \frac{\partial P_l}{\partial q_m^*}\frac{\partial q_m^*}{\partial z_j} = 0_{lj} \tag{A.3}$$

and solving for $\partial q_m^*/z_j$:

$$\frac{\partial P_l}{\partial q_m}\frac{\partial q_m^*}{\partial z_j} = -\frac{\partial P_l}{\partial z_j} \tag{A.4}$$

$$R_{kl}\frac{\partial P_l}{\partial q_m}\frac{\partial q_m^*}{\partial z_j} = -R_{kl}\frac{\partial P_l}{\partial z_j} \tag{A.5}$$

$$\frac{\partial q_k^*}{\partial z_j} = -R_{kl}\frac{\partial P_l}{\partial z_j} \tag{A.6}$$

where R is the left inverse matrix:

$$\delta_{km} = R_{kl}\frac{\partial P_l}{\partial q_m} \tag{A.7}$$

$$= R_{kl}\frac{\partial^2 \mathcal{F}}{\partial q_l \partial q_m} \tag{A.8}$$

The relaxed physical properties evaluated at constant T are then determined by repeated application of the chain rule:

$$\frac{\partial \mathcal{F}^*}{\partial z_i} = \frac{\partial \mathcal{F}}{\partial z_i} + \frac{\partial \mathcal{F}}{\partial q_k}\frac{\partial q_k^*}{\partial z_i} \tag{A.9}$$

$$= \frac{\partial \mathcal{F}}{\partial z_i} \tag{A.10}$$

where the second term in the first expression vanished by the requirement that $\partial\mathcal{F}/\partial q_k = 0_k$ at equilibrium (Equation A.2). Differentiating again yields

$$\frac{\partial^2\mathcal{F}^*}{\partial z_i \partial z_j} = \frac{\partial^2\mathcal{F}}{\partial z_i \partial z_j} + \frac{\partial^2\mathcal{F}}{\partial z_i \partial q_k}\frac{\partial q_k^*}{\partial z_j} \tag{A.11}$$

$$= \frac{\partial^2\mathcal{F}}{\partial z_i \partial z_j} - \frac{\partial^2\mathcal{F}}{\partial z_i \partial q_k} R_{kl} \frac{\partial^2\mathcal{F}}{\partial q_l \partial z_j} \tag{A.12}$$

$$\left[\begin{array}{c|c} V\mathbb{C}_{\mathrm{T}}^* & V\boldsymbol{\pi}^* \\ \hline V\boldsymbol{\pi}^{*\mathrm{T}} & -C_{\boldsymbol{\varepsilon}}^*/T \end{array}\right]_{ij} = \left[\begin{array}{c|c} V\mathbb{C}_{\mathrm{T}} & V\boldsymbol{\pi} \\ \hline V\boldsymbol{\pi}^{\mathrm{T}} & -c_{\boldsymbol{\varepsilon}}/T \end{array}\right]_{ij} - \frac{\partial^2\mathcal{F}}{\partial z_i \partial q_k} R_{kl} \frac{\partial^2\mathcal{F}}{\partial q_l \partial z_j} \tag{A.13}$$

This expression is similar to the expression under fixed entropy constraints presented by Slonczewski & Thomas (1970), their Equation 26. The elements of the unrelaxed block matrix (first term on the RHS of the last equation) can be evaluated directly from the anisotropic equation of state. Expressions for $\partial^2\mathcal{F}/\partial\boldsymbol{q}\partial\boldsymbol{q}$ (Equation A.8) and $\partial^2\mathcal{F}/\partial\boldsymbol{q}\partial\boldsymbol{z}$ (Equation A.13) can be derived by change of variables (Appendix B).

APPENDIX B: CHANGE OF VARIABLES AND DERIVATIVES OF THE HELMHOLTZ ENERGY

Here, we derive the partial derivatives in Section 3.3.2 by change of variables. The variables required are:

$$\left(\frac{\partial^2\mathcal{F}}{\partial q_i \partial q_j}\right)_{\boldsymbol{M}_{\mathrm{ref}},\boldsymbol{\varepsilon},T,q_{k\neq i,k\neq j},\boldsymbol{x}}, \left(\frac{\partial^2\mathcal{F}}{\partial q_i \partial T}\right)_{\boldsymbol{M}_{\mathrm{ref}},\boldsymbol{\varepsilon},\boldsymbol{q}_{j\neq i},\boldsymbol{x}}, \left(\frac{\partial^2\mathcal{F}}{\partial q_i \partial \varepsilon_{kl}}\right)_{\boldsymbol{M}_{\mathrm{ref}},\boldsymbol{\varepsilon}_{mn\neq kl},T,q_{j\neq i},\boldsymbol{x}} \tag{B.1}$$

where $\boldsymbol{M}_{\mathrm{ref}}$ is a constant reference cell tensor about which small strains can be performed. The equation of state developed by Myhill (2024) gives the partial derivatives of $\mathcal{F}(f', T', \boldsymbol{n}', \bar{\boldsymbol{\varepsilon}}')$, where $f = \ln V$. The "primes" are used to specify the variables of the equation of state. Making explicit the dependences on the variables in B.1, we have:

$$\mathcal{F} = \mathcal{F}(f'(\boldsymbol{M}_{\mathrm{ref}}, \boldsymbol{\varepsilon}), T'(T), \boldsymbol{n}'(\boldsymbol{q}, \boldsymbol{x}), \bar{\boldsymbol{\varepsilon}}'(\boldsymbol{M}_{\mathrm{ref}}, \boldsymbol{\varepsilon}, T, \boldsymbol{q}, \boldsymbol{x}))$$

The partial differential operators for the set of variables in B.1 are thus:

$$\frac{\partial}{\partial q_i} = \frac{\partial n'_u}{\partial q_i}\frac{\partial}{\partial n'_u} + \frac{\partial \bar{\varepsilon}'_{mn}}{\partial q_i}\frac{\partial}{\partial \bar{\varepsilon}'_{mn}} \tag{B.2}$$

$$\frac{\partial}{\partial T} = \frac{\partial}{\partial T'} + \frac{\partial \bar{\varepsilon}'_{pq}}{\partial T}\frac{\partial}{\partial \bar{\varepsilon}'_{pq}} \tag{B.3}$$

$$\frac{\partial}{\partial \varepsilon_{kl}} = \frac{\partial f'}{\partial \varepsilon_{kl}}\frac{\partial}{\partial f'} + \frac{\partial \bar{\varepsilon}'_{pq}}{\partial \varepsilon_{kl}}\frac{\partial}{\partial \bar{\varepsilon}'_{pq}} \tag{B.4}$$

In order to write the second derivatives in their most compact form, we first need to derive some of the partial derivatives in the three expressions above. These are:

- The constant stoichiometric ordering matrix:

$$\frac{\partial n'_i}{\partial q_j} = A_{ij} \tag{B.5}$$

- The small strain identity:

$$\frac{\partial f'}{\partial \varepsilon_{ij}} = \delta_{ij} \tag{B.6}$$

- Other derivatives are calculated considering the total derivative of the small strain tensor $\boldsymbol{\varepsilon}$:

$$d\varepsilon_{ij} = \frac{\partial \varepsilon_{ij}}{\partial f'} df' + \frac{\partial \varepsilon_{ij}}{\partial T'} dT' + \frac{\partial \varepsilon_{ij}}{\partial n'_k} dn'_k + \frac{\partial \varepsilon_{ij}}{\partial \bar{\varepsilon}'_{lm}} d\bar{\varepsilon}'_{lm} \tag{B.7}$$

- Taking the partial derivative with respect to ε_{kl} at constant T, $\boldsymbol{q}$ and $\boldsymbol{x}$:

$$\frac{\partial \bar{\varepsilon}'_{ij}}{\partial \varepsilon_{kl}} = \frac{\partial \varepsilon_{ij}}{\partial \varepsilon_{kl}} - \frac{\partial \varepsilon_{ij}}{\partial f'} \frac{\partial f'}{\partial \varepsilon_{kl}} = \delta_{ik}\delta_{jl} - \frac{\beta_{\mathrm{T}ij}}{\beta_{\mathrm{TR}}} \delta_{kl} \tag{B.8}$$

- with respect to q_i at constant $\boldsymbol{\varepsilon}$ $(= 0)$, T and $\boldsymbol{x}$:

$$\frac{\partial \bar{\varepsilon}'_{mn}}{\partial q_i} = -\frac{\partial \varepsilon_{mn}}{\partial n'_u} \frac{\partial n'_u}{\partial q_i} = -\frac{\partial \varepsilon_{mn}}{\partial n'_u} A_{ui} \tag{B.9}$$

- with respect to T at constant $\boldsymbol{\varepsilon}$ $(= 0)$, $\boldsymbol{q}$ and $\boldsymbol{x}$:

$$\frac{\partial \bar{\varepsilon}'_{mn}}{\partial T} = -\frac{\partial \varepsilon_{mn}}{\partial T'} = -\left(\frac{\alpha_{ij}}{\alpha_V} - \frac{\beta_{\mathrm{T}ij}}{\beta_{\mathrm{TR}}} \right) \alpha_V \tag{B.10}$$

- Assuming a hydrostatic reference state, we also have:

$$\frac{\partial \sigma_{ij}}{\partial X'} = -\delta_{ij} \frac{\partial P}{\partial X'} \text{ where } X \text{ could be } f', T' \text{ or } \boldsymbol{n}'. \tag{B.11}$$

$$\delta_{ij} \frac{\partial \varepsilon_{ij}}{\partial X'} = 0 \text{ where } X \text{ could be } T', \boldsymbol{n}' \text{ or } \bar{\boldsymbol{\varepsilon}}'. \tag{B.12}$$

Using these expressions, we can compactly write the second derivatives of interest:

$$\frac{\partial^2 \mathcal{F}}{\partial q_i \partial q_j} = \frac{\partial n'_u}{\partial q_i} \frac{\partial}{\partial n'_u} \left(\frac{\partial n'_v}{\partial q_j} \frac{\partial \mathcal{F}}{\partial n'_v} + \frac{\partial \bar{\varepsilon}'_{mn}}{\partial q_j} \frac{\partial \mathcal{F}}{\partial \bar{\varepsilon}'_{mn}} \right) + \frac{\partial \bar{\varepsilon}'_{mn}}{\partial q_i} \frac{\partial}{\partial \bar{\varepsilon}'_{mn}} \left(\frac{\partial n'_u}{\partial q_j} \frac{\partial \mathcal{F}}{\partial n'_u} + \frac{\partial \bar{\varepsilon}'_{pq}}{\partial q_j} \frac{\partial \mathcal{F}}{\partial \bar{\varepsilon}'_{pq}} \right) \tag{B.13}$$

$$= \frac{\partial n'_u}{\partial q_i} \left(\frac{\partial n'_v}{\partial q_j} \frac{\partial^2 \mathcal{F}}{\partial n'_u \partial n'_v} + \frac{\partial \bar{\varepsilon}'_{mn}}{\partial q_j} \frac{\partial^2 \mathcal{F}}{\partial n'_u \partial \bar{\varepsilon}'_{mn}} \right) + \frac{\partial \bar{\varepsilon}'_{mn}}{\partial q_i} \left(\frac{\partial n'_u}{\partial q_j} \frac{\partial^2 \mathcal{F}}{\partial n'_u \partial \bar{\varepsilon}'_{mn}} + \frac{\partial \bar{\varepsilon}'_{pq}}{\partial q_j} \frac{\partial^2 \mathcal{F}}{\partial \bar{\varepsilon}'_{pq} \partial \bar{\varepsilon}'_{mn}} \right) \tag{B.14}$$

$$= A_{ui} \left(A_{vj} H^{\mathcal{F}}_{uv} + \frac{\partial \bar{\varepsilon}'_{mn}}{\partial q_j} \frac{\partial \sigma_{mn}}{\partial n'_u} \right) + \frac{\partial \bar{\varepsilon}'_{mn}}{\partial q_i} \left(A_{uj} \frac{\partial \sigma_{mn}}{\partial n'_u} + \frac{\partial \bar{\varepsilon}'_{pq}}{\partial q_j} V \mathbb{C}_{\mathrm{T}mnpq} \right) \tag{B.15}$$

$$= A_{ui} \left(A_{vj} H^{\mathcal{F}}_{uv} + \frac{\partial \varepsilon_{mn}}{\partial n'_v} A_{vj} \delta_{mn} \frac{\partial P}{\partial n'_u} \right) - \frac{\partial \varepsilon_{mn}}{\partial n'_u} A_{ui} \left(-A_{vj} \delta_{mn} \frac{\partial P}{\partial n'_v} - \frac{\partial \varepsilon_{pq}}{\partial n'_v} A_{vj} V \mathbb{C}_{\mathrm{T}mnpq} \right) \tag{B.16}$$

$$= A_{ui} \left(H^{\mathcal{F}}_{uv} + V \frac{\partial \varepsilon_{mn}}{\partial n'_u} \mathbb{C}_{\mathrm{T}mnpq} \frac{\partial \varepsilon_{pq}}{\partial n'_v} \right) A_{vj} \tag{B.17}$$

$$\frac{\partial^2 \mathcal{F}}{\partial q_i \partial T} = \frac{\partial}{\partial T'}\left(\frac{\partial n'_u}{\partial q_i}\frac{\partial \mathcal{F}}{\partial n'_u} + \frac{\partial \bar{\varepsilon}'_{mn}}{\partial q_i}\frac{\partial \mathcal{F}}{\partial \bar{\varepsilon}'_{mn}}\right) + \frac{\partial \bar{\varepsilon}'_{pq}}{\partial T}\frac{\partial}{\partial \bar{\varepsilon}'_{pq}}\left(\frac{\partial n'_u}{\partial q_i}\frac{\partial \mathcal{F}}{\partial n'_u} + \frac{\partial \bar{\varepsilon}'_{mn}}{\partial q_i}\frac{\partial \mathcal{F}}{\partial \bar{\varepsilon}'_{mn}}\right) \tag{B.18}$$

$$= \left(\frac{\partial n'_u}{\partial q_i}\frac{\partial^2 \mathcal{F}}{\partial n'_u \partial T'} + \frac{\partial \bar{\varepsilon}'_{mn}}{\partial q_i}\frac{\partial^2 \mathcal{F}}{\partial \bar{\varepsilon}'_{mn}\partial T'}\right) + \frac{\partial \bar{\varepsilon}'_{pq}}{\partial T}\left(\frac{\partial n'_u}{\partial q_i}\frac{\partial^2 \mathcal{F}}{\partial n'_u \partial \bar{\varepsilon}'_{pq}} + \frac{\partial \bar{\varepsilon}'_{mn}}{\partial q_i}\frac{\partial^2 \mathcal{F}}{\partial \bar{\varepsilon}'_{mn}\partial \bar{\varepsilon}'_{pq}}\right) \tag{B.19}$$

$$= \left(-A_{ui}\frac{\partial N}{\partial n'_u} - \frac{\partial \varepsilon_{mn}}{\partial n'_i}A_{ui}V\frac{\partial \sigma_{mn}}{\partial T'}\right) - \frac{\partial \varepsilon_{pq}}{\partial T'}\left(A_{ui}V\frac{\partial \sigma_{pq}}{\partial n'_u} - \frac{\partial \bar{\varepsilon}'_{mn}}{\partial n'_u}A_{ui}V\mathbb{C}_{\mathrm{T}mnpq}\right) \tag{B.20}$$

$$= A_{ui}\left(-\frac{\partial N}{\partial n'_u} + V\frac{\partial \varepsilon_{mn}}{\partial n'_u}\mathbb{C}_{\mathrm{T}mnpq}\left(\frac{\alpha_{pq}}{\alpha_V} - \frac{\beta_{\mathrm{T}pq}}{\beta_{\mathrm{TR}}}\right)\alpha_V\right) \tag{B.21}$$

$$\frac{\partial^2 \mathcal{F}}{\partial q_i \partial \varepsilon_{kl}} = \frac{\partial f'}{\partial \varepsilon_{kl}}\frac{\partial}{\partial f'}\left(\frac{\partial n'_u}{\partial q_i}\frac{\partial \mathcal{F}}{\partial n'_u} + \frac{\partial \bar{\varepsilon}'_{mn}}{\partial q_i}\frac{\partial \mathcal{F}}{\partial \bar{\varepsilon}'_{mn}}\right) + \frac{\partial \bar{\varepsilon}'_{pq}}{\partial \varepsilon_{kl}}\frac{\partial}{\partial \bar{\varepsilon}'_{pq}}\left(\frac{\partial n'_u}{\partial q_i}\frac{\partial \mathcal{F}}{\partial n'_u} + \frac{\partial \bar{\varepsilon}'_{mn}}{\partial q_i}\frac{\partial \mathcal{F}}{\partial \bar{\varepsilon}'_{mn}}\right) \tag{B.22}$$

$$= \frac{\partial f'}{\partial \varepsilon_{kl}}\left(\frac{\partial n'_u}{\partial q_i}\frac{\partial^2 \mathcal{F}}{\partial n'_u \partial f'} + \frac{\partial \bar{\varepsilon}'_{mn}}{\partial q_i}\frac{\partial^2 \mathcal{F}}{\partial \bar{\varepsilon}'_{mn}\partial f'}\right) + \frac{\partial \bar{\varepsilon}'_{pq}}{\partial \varepsilon_{kl}}\left(\frac{\partial n'_u}{\partial q_i}\frac{\partial^2 \mathcal{F}}{\partial n'_u \partial \bar{\varepsilon}'_{pq}} + \frac{\partial \bar{\varepsilon}'_{mn}}{\partial q_i}\frac{\partial^2 \mathcal{F}}{\partial \bar{\varepsilon}'_{mn}\partial \bar{\varepsilon}'_{pq}}\right) \tag{B.23}$$

$$= A_{ui}\left(\delta_{kl}\left(-V\frac{\partial P}{\partial n'_u} - \frac{\partial \varepsilon_{mn}}{\partial n'_u}V\frac{\partial \sigma_{mn}}{\partial f'}\right) + \frac{\partial \bar{\varepsilon}'_{pq}}{\partial \varepsilon_{kl}}\left(V\frac{\partial \sigma_{pq}}{\partial n'_u} - \frac{\partial \varepsilon_{mn}}{\partial n'_u}V\mathbb{C}_{\mathrm{T}mnpq}\right)\right) \tag{B.24}$$

$$= -VA_{ui}\left(\delta_{kl}\frac{\partial P}{\partial n'_u} + \frac{\partial \varepsilon_{mn}}{\partial n'_u}\mathbb{C}_{\mathrm{T}mnpq}\left(\delta_{pk}\delta_{ql} - \frac{\beta_{\mathrm{T}pq}}{\beta_{\mathrm{TR}}}\delta_{kl}\right)\right) \tag{B.25}$$

APPENDIX C: CHANGE OF VARIABLES: COMPOSITIONAL DERIVATIVE OF THE CELL TENSOR

This appendix provides the first compositional derivative of the cell tensor under hydrostatic conditions $\boldsymbol{M}(V_{\mathrm{mol}}(V^\circ, \boldsymbol{n}^\circ), T(T^\circ), \boldsymbol{p}(\boldsymbol{n}^\circ), n(\boldsymbol{n}^\circ))$, where $^\circ$ denotes the required variable set:

$$\boldsymbol{M} = \boldsymbol{F}\boldsymbol{M}_0 \tag{C.1}$$

$$\ln_{\mathrm{M}} \boldsymbol{M}_0(\boldsymbol{p}, n) = p_m(\ln_{\mathrm{M}}(\boldsymbol{M}_{0m})) + \frac{\ln(n)}{3}\boldsymbol{I} \tag{C.2}$$

$$\ln_{\mathrm{M}} \boldsymbol{F}(V_{\mathrm{mol}}, T, \boldsymbol{p}) = (p_m \Psi_{ijklm}(V_{\mathrm{mol}}, T) + p_m p_n \mathbb{W}^{\Psi}_{ijklmn}(V_{\mathrm{mol}}, T, \boldsymbol{p}))\delta_{kl} \tag{C.3}$$

$$\text{where } V_{\mathrm{mol}} = \frac{V}{n},\ p_m = \frac{n_m}{n}, \text{ and } n = 1_l n_l \tag{C.4}$$

$$\text{so } \frac{\partial V_{\mathrm{mol}}}{\partial n^\circ_l} = -\frac{1_l V_{\mathrm{mol}}}{n},\ \frac{\partial n}{\partial n^\circ_l} = 1_l, \text{ and } = \frac{\partial p_m}{\partial n^\circ_l} = \left(\frac{n\delta_{lm} - 1_l n_m}{n^2}\right) = \left(\frac{\delta_{lm} - 1_l p_m}{n}\right) \tag{C.5}$$

Additionally, because $\boldsymbol{M_0 I} = \boldsymbol{I M_0}$, we can write

$$\frac{\partial M_{0kj}}{\partial n} = \frac{M_{0kj}}{3n^{2/3}}, \text{ and } \frac{\partial M_{0kj}}{\partial p_m} = n^{1/3}\frac{\partial M_{0\mathrm{mol}kj}}{\partial p_m} \tag{C.6}$$

$$\frac{\partial M_{ij}}{\partial n_l^\circ} = \frac{\partial F_{ik}}{\partial n_l^\circ} M_{0kj} + F_{ik} \frac{\partial M_{0kj}}{\partial n_l^\circ} \tag{C.7}$$

$$\frac{\partial F_{ik}}{\partial n_l^\circ} = \frac{\partial F_{ik}}{\partial V_{\text{mol}}} \frac{\partial V_{\text{mol}}}{\partial n_l^\circ} + \frac{\partial F_{ik}}{\partial p_m} \frac{\partial p_m}{\partial n_l^\circ} \tag{C.8}$$

$$= -\frac{\partial F_{ik}}{\partial V_{\text{mol}}} \frac{1_l V_{\text{mol}}}{n} + \frac{\partial F_{ik}}{\partial p_m} \left(\frac{\delta_{lm} - 1_l p_m}{n} \right) \tag{C.9}$$

$$\frac{\partial M_{0kj}}{\partial n_l^\circ} = \frac{\partial M_{0kj}}{\partial n} \frac{\partial n}{\partial n_l^\circ} + \frac{\partial M_{0kj}}{\partial p_m} \frac{\partial p_m}{\partial n_l^\circ} \tag{C.10}$$

$$= \frac{M_{0kj}}{3n^{2/3}} 1_l + \frac{\partial M_{0\text{mol}kj}}{\partial p_m} \left(\frac{\delta_{lm} - 1_l p_m}{n^{2/3}} \right) \tag{C.11}$$

APPENDIX D: CHANGE OF VARIABLES: SCALAR GIBBS DERIVATIVES TO HELMHOLTZ DERIVATIVES

This appendix provides partial differential operators and partial derivatives required to calculate the second order partial differentials of the Helmholtz energy $\mathcal{F}$ under hydrostatic conditions. As done for the Helmholtz energy under non-hydrostatic conditions in Appendix B, we define a set of variables for the hydrostatic Helmholtz energy $(V', T', \boldsymbol{n}')$, and a modified set for the hydrostatic Gibbs energy $(P^{\mathcal{G}}, T^{\mathcal{G}}, \boldsymbol{n}^{\mathcal{G}})$. Any function can then be written:

$$\Phi(P^{\mathcal{G}}(V', T', \boldsymbol{n}'), T^{\mathcal{G}}(T'), \boldsymbol{n}^{\mathcal{G}}(\boldsymbol{n}')) \tag{D.1}$$

The partial differential operators for the Helmholtz variables are:

$$\frac{\partial}{\partial V'} = \frac{\partial P}{\partial V'} \frac{\partial}{\partial P^{\mathcal{G}}} \tag{D.2}$$

$$\frac{\partial}{\partial T'} = \frac{\partial T}{\partial T'} \frac{\partial}{\partial T^{\mathcal{G}}} + \frac{\partial P}{\partial T'} \frac{\partial}{\partial P^{\mathcal{G}}} \tag{D.3}$$

$$\frac{\partial}{\partial n_i'} = \frac{\partial}{\partial n_i^{\mathcal{G}}} + \frac{\partial P}{\partial n_i'} \frac{\partial}{\partial P^{\mathcal{G}}} \tag{D.4}$$

In order to express the second derivatives in their most compact form, we will use the following thermodynamic identities:

$$\frac{\partial P}{\partial V} = -\frac{K_T}{V} \tag{D.5}$$

$$\frac{\partial P}{\partial T} = \frac{\partial N}{\partial V} = \alpha_V K_T \tag{D.6}$$

A final relation is obtained by taking the total derivative of V and differentiating with respect to $\boldsymbol{n}'$:

$$dV = \frac{\partial V}{\partial P^{\mathcal{G}}} dP^{\mathcal{G}} + \frac{\partial V}{\partial T^{\mathcal{G}}} dT^{\mathcal{G}} + \frac{\partial V}{\partial n_i^{\mathcal{G}}} dn_i^{\mathcal{G}} \tag{D.7}$$

$$\frac{\partial V}{\partial n'_j} = \frac{\partial V}{\partial P^{\mathcal{G}}} \frac{\partial P}{\partial n'_j} + \frac{\partial V}{\partial T^{\mathcal{G}}} \frac{\partial T}{\partial n'_j} + \frac{\partial V}{\partial n_i^{\mathcal{G}}} \frac{\partial n_i}{\partial n'_j} \tag{D.8}$$

$$0 = \frac{\partial V}{\partial P^{\mathcal{G}}} \frac{\partial P}{\partial n'_j} + \frac{\partial V}{\partial n_j^{\mathcal{G}}} \tag{D.9}$$

$$\frac{\partial P}{\partial n'_j} = -\frac{\partial P}{\partial V} \frac{\partial V}{\partial n_j^{\mathcal{G}}} \tag{D.10}$$

Finally, the required second derivatives can be derived:

$$\frac{\partial P}{\partial n'_i} = \frac{K_T}{V} \frac{\partial V}{\partial n_i^{\mathcal{G}}} \tag{D.11}$$

$$\frac{\partial N}{\partial n'_i} = \frac{\partial N}{\partial n_i^{\mathcal{G}}} + \frac{\partial P}{\partial n'_i} \frac{\partial N}{\partial P^{\mathcal{G}}} \tag{D.12}$$

$$= \frac{\partial N}{\partial n_i^{\mathcal{G}}} + \left(-\frac{\partial P}{\partial V} \frac{\partial V}{\partial n_i^{\mathcal{G}}} \right) \frac{\partial N}{\partial P^{\mathcal{G}}} \tag{D.13}$$

$$= \frac{\partial N}{\partial n_i^{\mathcal{G}}} - \alpha_V K_T \frac{\partial V}{\partial n_i^{\mathcal{G}}} \tag{D.14}$$

$$\frac{\partial^2 \mathcal{F}}{\partial n'_i \partial n'_j} = \frac{\partial^2 \mathcal{G}}{\partial n'_i \partial n'_j} - V \frac{\partial^2 P}{\partial n'_i \partial n'_j} \tag{D.15}$$

$$= \frac{\partial^2 \mathcal{G}}{\partial n_i^{\mathcal{G}} \partial n_j^{\mathcal{G}}} + \frac{\partial P}{\partial n'_i} \frac{\partial^2 \mathcal{G}}{\partial P^{\mathcal{G}} \partial n_j^{\mathcal{G}}} + \frac{\partial P}{\partial n'_j} \frac{\partial^2 \mathcal{G}}{\partial P^{\mathcal{G}} \partial n_i^{\mathcal{G}}} + \frac{\partial P}{\partial n'_i} \frac{\partial P}{\partial n_j} \frac{\partial^2 \mathcal{G}}{\partial P^{\mathcal{G}} \partial P^{\mathcal{G}}} \tag{D.16}$$

$$= \frac{\partial^2 \mathcal{G}}{\partial n_i^{\mathcal{G}} \partial n_j^{\mathcal{G}}} + \frac{\partial V}{\partial n_i^{\mathcal{G}}} \left(\frac{K_T}{V} \right) \frac{\partial V}{\partial n_j^{\mathcal{G}}} + \frac{\partial V}{\partial n_j^{\mathcal{G}}} \left(\frac{K_T}{V} \right) \frac{\partial V}{\partial n_i^{\mathcal{G}}} - \frac{\partial V}{\partial n_i^{\mathcal{G}}} \left(\frac{K_T}{V} \right) \frac{\partial V}{\partial n_j^{\mathcal{G}}} \tag{D.17}$$

$$= \frac{\partial^2 \mathcal{G}}{\partial n_i^{\mathcal{G}} \partial n_j^{\mathcal{G}}} + \frac{\partial V}{\partial n_i^{\mathcal{G}}} \left(\frac{K_T}{V} \right) \frac{\partial V}{\partial n_j^{\mathcal{G}}} \tag{D.18}$$

APPENDIX E: CHANGE OF VARIABLES: ANISOTROPIC HELMHOLTZ DERIVATIVES TO INTERNAL ENERGY DERIVATIVES

This appendix provides partial differential operators and partial derivatives required to calculate the second order partial differentials of the internal energy $\mathcal{E}$ as functions of partial derivatives of the Helmholtz energy $\mathcal{F}$. We define a "natural" set of variables for the Helmholtz energy in the small strain case $(\boldsymbol{\varepsilon}, T, \boldsymbol{n})$, and a modified set for the internal energy $(\boldsymbol{\varepsilon}^{\mathcal{E}}, N^{\mathcal{E}}, \boldsymbol{n}^{\mathcal{E}})$. Any function can be written

$$\Phi(\boldsymbol{\varepsilon}(\boldsymbol{\varepsilon}^{\mathcal{E}}), T(\boldsymbol{\varepsilon}^{\mathcal{E}}, N^{\mathcal{E}}, \boldsymbol{n}^{\mathcal{E}}), \boldsymbol{n}(\boldsymbol{n}^{\mathcal{E}})) \tag{E.1}$$

The partial differential operators for the modified set of variables are:

$$\frac{\partial}{\partial \varepsilon_{ij}^{\mathcal{E}}} = \delta_{ik}\delta_{jl}\frac{\partial}{\partial \varepsilon_{kl}} + \frac{\partial T}{\partial \varepsilon_{ij}^{\mathcal{E}}}\frac{\partial}{\partial T} \tag{E.2}$$

$$\frac{\partial}{\partial N^{\mathcal{E}}} = \frac{\partial T}{\partial N^{\mathcal{E}}}\frac{\partial}{\partial T} \tag{E.3}$$

$$\frac{\partial}{\partial n_i^{\mathcal{E}}} = \delta_{ij}\frac{\partial}{\partial n_j} + \frac{\partial T}{\partial n_i^{\mathcal{E}}}\frac{\partial}{\partial T} \tag{E.4}$$

In order to express the second derivatives in their most compact form, we will use the following thermodynamic identity:

$$\frac{\partial T}{\partial N} = \frac{c_\varepsilon}{T} \tag{E.5}$$

Further relations are obtained by differentiating N with respect to the $\boldsymbol{\varepsilon}^{\mathcal{E}}$, $N^{\mathcal{E}}$ and $\boldsymbol{x}^{\mathcal{E}}$:

$$dN = \frac{\partial N}{\partial \varepsilon_{ij}}d\varepsilon_{ij} + \frac{\partial N}{\partial T}dT + \frac{\partial N}{\partial n_i}dn_i \tag{E.6}$$

$$\frac{\partial T}{\partial \varepsilon_{ij}^{\mathcal{E}}} = -\frac{T}{c_\varepsilon}\frac{\partial N}{\partial \varepsilon_{ij}} \tag{E.7}$$

$$\frac{\partial T}{\partial N^{\mathcal{E}}} = \frac{c_\varepsilon}{T} \tag{E.8}$$

$$\frac{\partial T}{\partial n_i^{\mathcal{E}}} = -\frac{T}{c_\varepsilon}\frac{\partial N}{\partial n_i} \tag{E.9}$$

Finally, the required second derivatives can be derived:

$$\frac{\partial^2 \mathcal{E}}{\partial n_i^{\mathcal{E}}\partial N^{\mathcal{E}}} = \frac{\partial T}{\partial n_i^{\mathcal{E}}} = -\frac{T}{c_\varepsilon}\frac{\partial N}{\partial n_i} = \frac{T}{c_\varepsilon}\frac{\partial^2 \mathcal{F}}{\partial n_i \partial T} \tag{E.10}$$

$$\frac{\partial^2 \mathcal{E}}{\partial n_i^{\mathcal{E}}\partial \varepsilon_{jk}^{\mathcal{E}}} = \frac{\partial \sigma_{jk}}{\partial n_i^{\mathcal{E}}} = \frac{\partial^2 \mathcal{F}}{\partial n_i \partial \varepsilon_{jk}} - \frac{T}{c_\varepsilon}\frac{\partial N}{\partial n_i}\frac{\partial^2 \mathcal{F}}{\partial T \partial \varepsilon_{jk}} = \frac{\partial^2 \mathcal{F}}{\partial n_i \partial \varepsilon_{jk}} + \frac{VT\pi_{jk}}{c_\varepsilon}\frac{\partial^2 \mathcal{F}}{\partial n_i \partial T} \tag{E.11}$$

$$\frac{\partial^2 \mathcal{E}}{\partial n_i^{\mathcal{E}}\partial n_j^{\mathcal{E}}} = \frac{\partial^2 \mathcal{F}}{\partial n_i^{\mathcal{E}}\partial n_j^{\mathcal{E}}} + N\frac{\partial^2 T}{\partial n_i^{\mathcal{E}}\partial n_j^{\mathcal{E}}} \tag{E.12}$$

$$= \frac{\partial^2 \mathcal{F}}{\partial n_i \partial n_j} + \frac{\partial T}{\partial n_i^{\mathcal{E}}}\frac{\partial^2 \mathcal{F}}{\partial n_j \partial T} + \frac{\partial T}{\partial n_j^{\mathcal{E}}}\frac{\partial^2 \mathcal{F}}{\partial n_i \partial T} + \frac{\partial T}{\partial n_i^{\mathcal{E}}}\frac{\partial^2 \mathcal{F}}{\partial T \partial T}\frac{\partial T}{\partial n_j^{\mathcal{E}}} \tag{E.13}$$

$$= \frac{\partial^2 \mathcal{F}}{\partial n_i \partial n_j} + \frac{\partial T}{\partial n_i^{\mathcal{E}}}\frac{\partial^2 \mathcal{F}}{\partial n_j \partial T} + \frac{\partial T}{\partial n_j^{\mathcal{E}}}\frac{\partial^2 \mathcal{F}}{\partial n_i \partial T} - \frac{\partial T}{\partial n_i^{\mathcal{E}}}\frac{\partial N}{\partial T}\frac{\partial T}{\partial n_j^{\mathcal{E}}} \tag{E.14}$$

$$= \frac{\partial^2 \mathcal{F}}{\partial n_i \partial n_j} + \frac{T}{c_\varepsilon}\frac{\partial N}{\partial n_i}\frac{\partial N}{\partial n_j} + \frac{T}{c_\varepsilon}\frac{\partial N}{\partial n_j}\frac{\partial N}{\partial n_i} - \frac{T}{c_\varepsilon}\frac{\partial N}{\partial n_j}\frac{\partial N}{\partial n_i} \tag{E.15}$$

$$= \frac{\partial^2 \mathcal{F}}{\partial n_i \partial n_j} + \frac{\partial N}{\partial n_i}\frac{T}{c_\varepsilon}\frac{\partial N}{\partial n_j} \tag{E.16}$$

$$= \frac{\partial^2 \mathcal{F}}{\partial n_i \partial n_j} + \frac{\partial^2 \mathcal{F}}{\partial n_i \partial T}\frac{T}{c_\varepsilon}\frac{\partial^2 \mathcal{F}}{\partial n_j \partial T} \tag{E.17}$$

This paper has been produced using the Blackwell Scientific Publications GJI LaTeX2e class file.